DOE/ER/45056-10

"Energy Transfer and Non-linear Optical Properties at Near Ultraviolet Wavelengths: Rare Earth 4f→5d Transitions in Crystals and Glasses"

FINAL REPORT

DOE/ER/45056--10

DE93 002133

for the period June 1, 1984 to May 31, 1992

Douglas S. Hamilton
Associate Professor
Department of Physics
and
Institute of Materials Science
University of Connecticut
Storrs, Connecticut 06269-3046

August 1992

Prepared for
The United States Department of Energy
Office of Basic Energy Sciences
Department of Materials Sciences

Grant No. DE-FG02-84ER45056

CONTENTS

I. INTRODUCTION

The project has considered the optical properties of lanthanide (rare-earth) doped crystals and glasses at near ultraviolet wavelengths. These include two-photon absorption, excited state absorption, excited-state photoionization and color center formation, two-step photoconductivity, optical gain, energy transfer, nonradiative relaxation and optical grating formation.

Two-photon absorption (TPA) is the most fundamental nonlinear optical process. We have completed measurements of the TPA spectra and its polarization dependance for the 4f→5d transitions of Ce^{3+}:CaF_2. A detailed theoretical treatment of TPA in this material has been developed and is compared to the experimental measurements.

Excited state absorption (ESA) is a potential loss mechanism for all solid state lasers. This is specially so in Ce:YAG where we have measured a peak ESA cross-section of 1×10^{-17} cm^2. The shape of the ESA spectra and the magnitude of the cross section is consistent with a photoionization process. Two-step photoconductivity experiments confirmed the assignment of the conduction band as the terminal state of the ESA transition. Strong probe saturation measurements were used to investigate the dynamics and recovery processes in the excited state.

Optical pumping of Ce^{3+}:CaF_2 at 308 nm leads to a two-photon photoionization and the subsequent creation of photochromic color centers. A one-photon photobleaching of these centers and the finite electron acceptor density leads to a complex, but solvable rate equation for the number of color centers. The electron acceptors are trivalent cerium ions at quasi-cubic sites, which become divalent following the electron capture. The photo-bleaching involves the photoionization of the divalent cerium ions, with the electron returning to the original tetragonal symmetry site. Thermoluminescence measurements are used to study the thermally activated recombination radiation.

Measurements of the optical gain and loss at 325 nm in Ce^{3+}:LiYF4 are presented. In addition to creating a cerium ion population inversion, the ultraviolet pumping at 308 nm forms transient and stable color centers via the excited cerium states. These color centers have absorption bands which overlap the cerium emission bands, and thus reduce the stimulated gain.

The repetition rate of a Ce^{3+}:$LiYF_4$ laser is limited to 0.5 Hz due to the relaxation rate of the transient centers.

Crystals of Cr^{3+}:GSGG, Cr^{3+}:GSAG and Cr^{3+}:GGG show several sharp absorption lines in the 310 nm to 340 nm region which we have identified as transitions of the Gd^{3+} ion. Excitation spectra taken by monitoring the Cr^{3+} luminescence shows that a rapid $Gd^{3+} \rightarrow Cr^{3+}$ energy transfer process is active in this material. Measurements of the time dependance of the Cr^{3+} fluorescence following pulsed laser excitation of the Gd^{3+} ions indicates the characteristic time over which this energy transfer occurs. By comparing measurements at 300 K with those at 77 K, the energy transfer process is seen to have a weak temperature dependance.

The 5d→4f transitions of cerium doped crystals are generally thought to have unity quantum efficiency of luminescence at room temperature. However, at higher temperatures, nonradiative processes which depopulate the 5d level become active. Measurements of the lifetimes of the 5d→4f fluorescence transitions in Ce^{3+}:CaF_2, Ce^{3+}:$LiYF_4$, Ce^{3+}:LaF_3, Ce^{3+}:$Y_3Al_5O_{12}$, Ce^{3+}:$YAlO_3$, Ce^{3+}:YPO_4 Ce^{3+}:fluoroberyllate glass, and Ce^{3+}:silicate glass between 77 K and 1,200 K are used to evaluate the nonradiative relaxation rates. A tentative model for the nonradiative relaxation involves thermal promotion to higher conduction band states.

A He-Cd laser at 442 nm has been used to write cw grating structures in Ce^{3+}:$Y_3Al_5O_{12}$. Observation of the spatially modulated fluorescence pattern from the excited Ce^{3+} ions indicate that little spatial energy transfer occurs for a 0.05% Ce^{3+} concentration over distances greater than 10 μ. In Ce^{3+}:CaF_2, permanent gratings have been created using a 308 nm XeCl laser beam to photoionize the Ce^{3+} ions and a 442 nm He-Cd beams to write the grating by a photobleaching process.

These research projects are considered in more detail in the following section. We then list the publications, conference presentations and thesis which have been completed under the auspices of this grant. A summary of the personnel supported by this grant and their accomplishments is then presented.

II. RESEARCH PROJECTS

A. Two photon transitions from the 4f ground state to the 5d excited states in Ce^{3+}:CaF_2

*The research summarized in this section has been published in 2 journal articles ["Two-photon Excitations of Higher 5d States in Ce^{3+}:CaF_2," S.K. Gayen, G.J. Pogatshnik and D.S. Hamilton, J. Lumin. **31/32**, 260 (1984), "Analysis of the Lowest 4f→5d Two-photon Transition in Ce^{3+}:CaF_2," S.K. Gayen, D.S. Hamilton and R.H. Bartram, Phys. Rev. B **34**, 7517 (1986)], presented at 1 conference [International Luminescence Conference, Madison, Wisconsin, 1984] and formed part of the Ph.D. thesis of Swapan K. Gayen.*

Two-photon absorption (TPA) is the most fundamental nonlinear optical process in an impurity doped solid. In TPA, a photon of frequency ν_1 and a second photon of frequency ν_2 are simultaneously absorbed by the impurity ion which results in a transition to a state with energy $\Delta E = (\nu_1+\nu_2)/h$. Although the process can be resonantly enhanced by an intermediate state, it is distinct from excited-state absorption where one of the two photons is used to populate this intermediate state. The selection rules for TPA are complementary to those for one-photon absorption. Thus for a 4f→5d transition on a lanthanide ion, the transition is electric-dipole allowed for a one-photon process but forbidden for a two-photon process. The selection rule can be partially lifted by the crystal-field mixing of states of opposite parity into either the initial (4f) or final state (5d). This mixing is similar to that used to describe the 4f→4f one photon transitions in the lanthanides. Although TPA in rare-earth ion doped solids has been extensively studied for the sharp 4f→4f no-phonon transitions, little experimental[1-3] or theoretical[3,4] work has been done on the first-order parity forbidden 4f→5d TPA transitions. It is these considerations which motivated our experimental and theoretical studies of TPA in Ce^{3+}:CaF_2.

The technique used to investigate TPA is that of excitation spectroscopy where the intensity of the 4f→5d fluorescence is measured as the wavelength of the exciting light is varied. A wavelength tunable dye laser pumped by a Q-switched Nd:YAG laser was used to generate the exciting light. Computer controlled instrumentation was used to normalize the signal by the square of the dye laser intensity. The two-photon excitation spectrum displayed in Fig. A1 is

from the lowest Stark component of the $^2F_{5/2}$ manifold to the lowest of the 5d states. The sharp zero-phonon line at the low energy end of the spectrum is the purely electronic transition between the two states. The appearance of the zero-phonon line in the TPA spectrum of this first-order parity-forbidden two-photon transition may be explained in terms of the crystal-field parity mixing among the participating states. Since the Ce^{3+} ion is at a site which lacks a center of inversion, the crystal field can mix the 5d states with the 4f ground state, and the 4f states with the lowest 5d state. The parity selection rule is thus relaxed, and a two-photon transition between mixed-parity states becomes possible. The measured peak value of the TPA cross section for the zero-phonon transition is of the order 10^{-54} cm^4sec, which indicates that the odd–parity component of the C_{4v} field is very effective in mixing the required states of opposite parity.

The TPA cross section for the zero-phonon transition shows a strong dependence on the polarization direction of the incident laser beam as noted in Fig. A2. Measurements of the polarization anisotropy of the TPA cross section for the zero-phonon transition and its analysis following the general group-theoretical formalism confirm the C_{4v} symmetry of the cerium site, and reveal that for the case of two identical photons, only A_1 and E symmetry transitions contribute to the total TPA transition probability. For a laser beam incident along the [100] axis of the CaF_2 host, the TPA cross section as a function of the polarization direction is given by the relation[1]

$$\sigma(\theta) = a + b\sin^2(2\theta), \tag{A1}$$

where θ is the angle between the polarization vector and the [010] axis, and a and b are functions of both the photon frequency and the matrix elements between the states participating in the transition. The polarization anisotropy,

$$A = \frac{\sigma(45°)-\sigma(0°)}{\sigma(45°)+\sigma(0°)}, \tag{A2}$$

is 0.50 for the zero-phonon transition.

The theoretical description of TPA in an impurity-ion doped solid begins with the expression for the TPA cross section per photon per ion in the electric-dipole approximation is

$$\sigma = \frac{4\pi^2 e^4}{h^2 c^3} (\eta_1 \eta_2)^2 \, L(\nu) \times \left| \sum_i \left[\frac{\langle f|\hat{e}_1 \cdot \mathbf{r}|i\rangle\langle i|\hat{e}_2 \cdot \mathbf{r}|g\rangle}{\nu_{ig} - \nu_2} + \frac{\langle f|\hat{e}_2 \cdot \mathbf{r}|i\rangle\langle i|\hat{e}_1 \cdot \mathbf{r}|g\rangle}{\nu_{ig} - \nu_1} \right] \right|^2 \qquad \text{A(3)}$$

where $|g\rangle$, $|i\rangle$ and $|f\rangle$ are the ground, intermediate and final states of the transition, $L(\nu)$ is the normalized lineshape function and ν_{ig} is the ground to intermediate state splitting in cm^{-1}. The subscripts 1 and 2 denote the particular photon with a frequency in cm^{-1} of ν and a polarization unit vector of $\hat{e}$. The index of refraction at that frequency is n and the local field correction is η.

Our evaluation of this expression involves two major steps.[3,4] The first is the calculation of the mixing of the 4f and 5d states by the odd parity crystal field which couple to the Ce^{3+} ion in a site of tetragonal (C_{4v}) symmetry. This process results in the appropriate wave functions $|g\rangle$ and $|f\rangle$ of the ground and final states respectively.

The second step involves the use of a closure approximation in order to evaluate the sum over intermediate states appearing in Eq. (A3). Assuming a constant energy denominator ($\nu - \nu_{ig} = \Delta$ for all $|i\rangle$) and evaluating Eq. A3 for the case of two identical photons with polarization $\hat{e}$, we have

$$\sigma = \frac{16\pi^2 n^2 e^4 \eta^4}{n^2 h^2 c^3} \frac{\left| \langle f|(\hat{e} \cdot \mathbf{r})^2|g\rangle \right|^2}{\Delta^2} L(\nu) \, . \qquad \text{(A4)}$$

Matrix elements between radial wavefunctions of the form $\langle R_{4f}|r^2|R_{4f}\rangle$ and $\langle R_{5d}|r^2|R_{5d}\rangle$ were calculated from Fischer's multiconfiguration Hartree-Fock program.[5] Using values of $\eta = (n^2+2)/3$, where n=1.43; ν=15964 cm^{-1} for excitation of the zero-phonon transition; Δ=40000 cm^{-1}; and $L(\nu) = (FWHM)^{-1} = (0.64 cm^{-1})^{-1}$ for the zero-phonon transition, we have

$$\sigma(0°) = (1/\varepsilon^2)\, 2.67\times10^{-49} \text{ cm}^4 \text{ sec}$$

$$\sigma(45°) = (1/\varepsilon^2)\, 3.11\times10^{-49} \text{ cm}^4 \text{ sec.} \qquad \text{(A5)}$$

In this work we have developed a second-order perturbation theory to calculate the two-photon absorption cross section for the lowest 4f→5d no-phonon transition in Ce^{3+}:CaF_2. In order to compare the results of this calculation to those obtained experimentally, we first consider the value of the polarization anisotropy defined by Eq.(A2). Since it involves a ratio, and is thus independent of any overall scale factors, it is more amenable to both accurate calculation and measurement than is the absolute cross section itself. Nevertheless, the measured anisotropy is 0.5 whereas, using the cross sections from Eq.(A4), the calculated anisotropy factor is only 0.076. Although the calulated value has the correct sign, it gives a much more isotropic polarization dependence to the cross section than is measured.

A much more difficult comparison to make is that for the absolute magnitudes of the TPA cross sections. The electrostatic screening of the optically active electron on the cerium ion from the electric field of the F^- charge compensator has been incorporated phenomenologically into the dielectric constant ε. This includes both the screening due to the ligands as well as the very strong shielding of the 4f electron by the filled 5s and 5p cerium orbitals and the somewhat weaker shielding of the 5d electron. A value of ε=365 would be required to bring the value of the calculated cross section into agreement with the measured value. The static dielectric constant of CaF_2 is 7.36 which leaves about a factor of 50 to be accounted for by the Sternheimer-shielding[6] of the 4f electron. Given the factor-of-five uncertainty in the measured cross section and the strength of this 4f electron screening in other trivalent-rare-earth ions, there is a reasonable agreement between the measured and calculated cross sections.

In order to account for the discrepancy between the experimental results and theoretical estimates, especially that for the polarization anisotropy, one may question the adequacy of the closure approximation. However, there are no intermediate states in near resonance with the photon frequency for which the energy denominator is small. For the 4f and 5d states in Ce^{3+}:CaF_2, the value of the energy denominator varies from 12400 cm^{-1} to about 37400 cm^{-1},while for the 6s and conduction band states, the value is somewhat higher. Thus the closure approximation is not too severe in this case and the inadequacy of the theory must be elsewhere.

In order to account for the integrated intensities and polarization anisotropy of the 4f→4f transition in Gd^{3+}:LaF_3 measured by Dagenais *et al.*[7], third-order perturbation terms involving spin orbit interaction among the levels of the intermediate configurations were introduced by Judd and Pooler.[8] Additional TPA measurements on this system by Downer *et al.*[9] gave results which could only be explained by invoking third and fourth-order terms involving spin-orbit and/or crystal field interactions among levels of the intermediate configuration. The contributions of these higher order terms were found to be comparable to or even higher than those from the second-order terms. Thus the possibility of obtaining better agreement with experiment for the polarization anisotropy in Ce^{3+}:CaF_2 by using higher orders in perturbation theory cannot be ruled out. Since these higher order terms involve levels of the same configuration, the additional energy denominators that enter into the expression for the cross section will be small for the 4f intermediate states in Ce^{3+}:CaF_2 and the corresponding contributions to the cross section may be large. As was in the case for the 4f→4f TPA transitions in Gd^{3+}:LaF_3, the inclusion of higher order terms may reproduce the correct magnitude of the polarization anisotropy. However, that may increase the value of the cross section as was seen in Gd^{3+}:LaF_3. It is possible however, to have destructive interference between the second order and higher order contributions which would reduce the magnitude of the cross section.

The polarization anisotropy of the TPA cross section is sensitive to the initial, final and intermediate wave functions being used. In this calculation, as well as in the second-order theory of Axe[10] and in the higher-order theories of Judd and Pooler[8] and Downer and Bivas[11], the participating states are all constructed from electronic configurations localized on the rare-earth ion. However, ligand dependent effects may make significant additional contributions to the TPA cross section. There may be a small overlap between the Ce^{3+} 5d wave functions and the wave functions of the charge compensator and other ligands. This covalency can play a role in creating mixed parity states. Recently Reid and Richardson[12] have shown that radiation-induced ligand polarization (also called dynamic ligand polarization) may make a significant contribution

to the TPA strengths. These authors considered the 4f→4f TPA transitions for the rare-earth ions and studied the contribution of dynamic ligand polarization to a third or fourth-order TPA intensity analysis. They argued that the inclusion of this effect in the calculation leads to two different sets of intermediate states; one consisting of ligand excited states and the other includes the $4f^{N-1}5d$ states of the rare-earth ion. Their conclusion was that a third-order process involving ligand excited states makes a contribution to the cross section which is comparable to that from the static crystal filed in third order. Dynamic ligand polarization may make a significant contribution to the TPA cross section in Ce^{3+}:CaF_2 as well, and any future higher-order calculation should incorporate this effect.

In this work we have calculated the magnitude of the TPA cross section and its polarization anisotropy for the zero-phonon transition alone. The phonon sideband shows a frequency-dependent polarization anisotropy, which is an intrinsic feature of the Ce^{3+}:CaF_2 system, and may be expected in similar systems, For an allowed TPA transition and also for the 4f→5d TPA transition in Eu^{2+}:CaF_2 where the ion is at a site of inversion symmetry, the phonon sideband has the same polarization anisotropy as would be expected of a purely electronic transition in the system under study. The Ce^{3+} ion in CaF_2 is at a site which lacks inversion symmetry and hence both even and odd vibrational modes may appear in the phonon sideband for the two-photon transition. It is this superposition of the crystal field and the vibronically induced transitions which gives the phonon sideband its frequency dependent polarization anisotropy. A detailed quantitative analysis of this frequency dependence presents an interesting and challenging problem for further investigation.

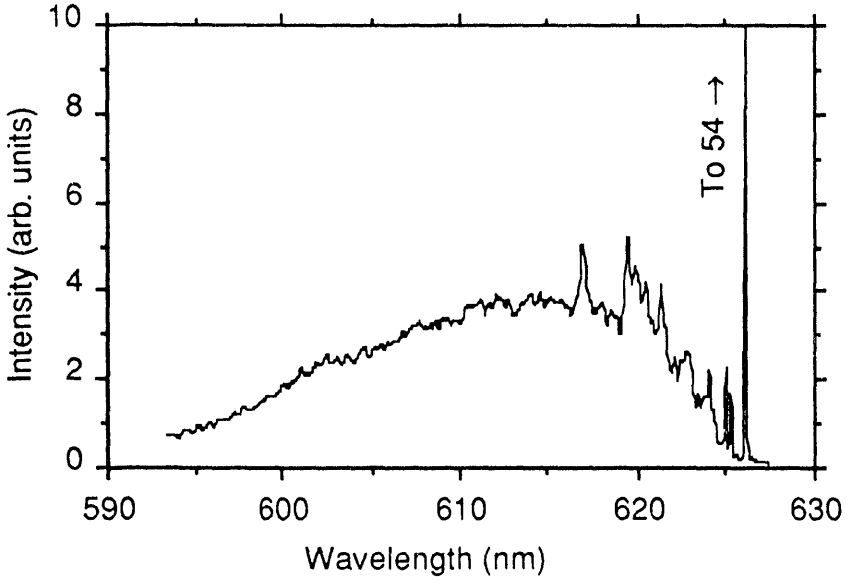

Figure A1. Composite two-photon excitation spectrum of 0.003 at% Ce^{3+}:CaF_2 at 6K. The fluorescence intensity has been point-by-point normalized to the square of the dye=laser power. The dye laser beam is along the [100] axis and is linearly polarized 45° to the [010] axis.

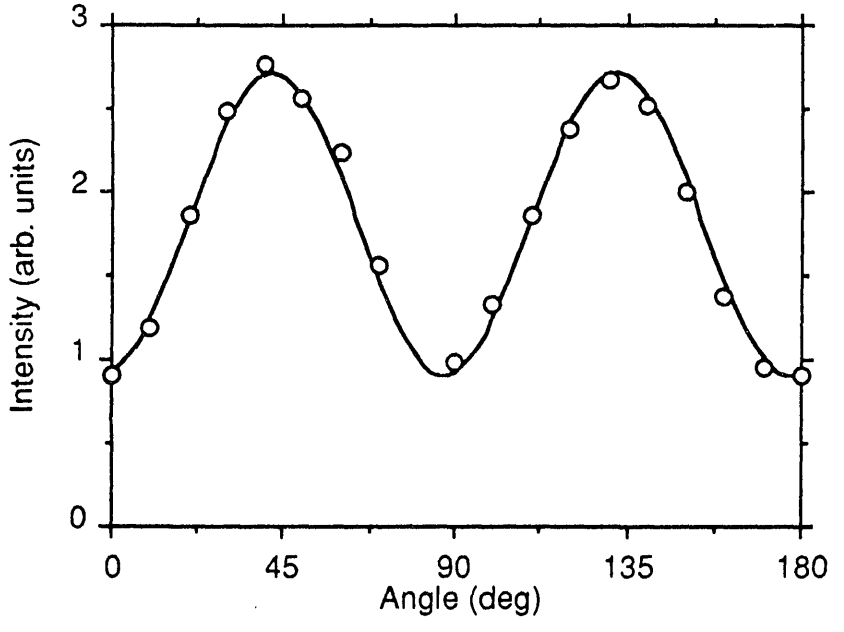

Figure A2. Polarization dependence of the two-photon absorption cross-section for the zero-phonon transition at a 6-K sample temperature. The dye laser beam is incident along the [100] axis and the angle θ is measured from the [010] axis of the host crystal. The circles represent the experimental measurments and the curve is a fit to the data using the angular function of Eq. (A2).

B. Optical absorption and photoionization studies in the excited states of $Ce^{3+}:Y_3Al_5O_{12}$

The research summarized in this section has been published in 2 journal articles ["Optical Absorption and Photoionization Measurements from the Excited States of $Ce^{3+}:Y_3Al_5O_{12}$," D.S. Hamilton, S.K. Gayen, G.J. Pogatshnik, R.D. Ghen and W.J. Miniscalco, Phys. Rev B 39,8807 (1989), "Trivalent Cerium as Tunable Laser Systems: Two Bad Apples," D.S. Hamilton, in Tunable Solid State Lasers, Vol. 47 of Springer Series in Optical Sciences, ed. by P. Hammerling, A. Budgor and A. Pinto, (Springer-Verlag, Berlin, 1985), pp. 80–90.], and presented at 2 conferences [March 1984 Meeting of the American Physical Society, Tunable Solid State Lasers Conference, La Jolla, California, 1984].

The usual optical characteristics of $Ce^{3+}:Y_3Al_5O_{12}$ (YAG) would suggest that this material would be an ideal wavelength tunable solid state laser. Operating on the 5d→4f transition of the Ce^{3+} ion, the fluorescence spectra indicates a potential tuning range from about 500 to 650 nm. The fluorescence lifetime is 65 ns and has a near unity quantum efficiency. The broad pump bands have large oscillator strengths and the YAG host has well-characterized thermal and optical characteristics. However, Ce:YAG suffers from the detrimental effects of excited state absorption (ESA), which is sufficiently strong to completely quench any possible laser action.[13-17] Since Ce^{3+}:YAG is a prototypic laser material operating on the 5d→4f transition of a trivalent rare-earth ion, it was important to fully understand the ESA and its deleterious role in determining the laser potential of Ce^{3+}:YAG.

The excitation source for populating the lowest 5d level was a tunable dye laser pumped by a 308 nm XeCl excimer laser (Quanta–Ray EXC–1). At a wavelength of 500 nm, the excitation was into the low–energy tail of the lowest 4f→5d absorption where the ground state absorption coefficient was measured to be α=9.0 cm^{-1}. Excitation at this wavelength results in a minimal thermal loading of the crystal and a convenient penetration depth of the pump beam. By placing an additional mirror at the excimer laser output, we were also able to pump into the high–energy tail of the second 5d level with the 308 nm beam. A second dye laser, pumped by the second harmonic of a Nd:YAG laser (Quanta–Ray DCR–1) generated the probe beam.

The sample cell for the photoconductivity measurements was of a blocking electrode design where the electrodes are not in direct contact with the sample.[18] The two–step photoconductivity was measured using two dye lasers pumped by the second and third harmonics of a Nd:YAG laser. The first dye laser was operated at 460 nm, which corresponds to the peak of the 4f to lowest–5d absorption. The second dye laser beam with a 700 nm wavelength was delayed by 10 ns with respect to the arrival of the first dye laser pulse. The resulting photocurrent was measured by a Keithley 610C electrometer. The 0.5 mole % Ce^{3+}:YAG samples used were Czochralski grown by Airtron Inc. For the ESA measurements, a polished $3\times3\times6$ mm^3 sample was used with a 3 mm absorption path length. The photoconductivity measurements were done with a 6 mm diameter by 0.15 mm thick disk–shaped sample.

For a coaxial pump-probe geometry using two pulsed lasers, the ESA cross-section is related to the experimental parameters by[17]

$$\alpha^* L = \ln\left(\frac{n(0)}{n(L)}\right) = \sigma^* N(0)\, e^{-t'/\tau}\, (1-e^{-\alpha L})\, \beta\, W, \qquad \text{(B1)}$$

where α^* is the ESA coefficient, L is the sample thickness, t' the pump-to-probe delay, τ the excited state lifetime, a the ground state absorption coefficient, β the pumping quantum efficiency, W the overlap integral of the pump and probe spatial profiles and n(0) and n(L) are the number of incident and transmitted probe photons respectively.

We have used this same coaxial beam geometry for the two–step photoconductivity measurements.[17,18] An equation for the photoresponse can be derived for a cell which utilizes a pair of blocking electrodes,

$$\Delta Q = \frac{\eta n(0)}{AL}(1-e^{-\alpha^* L})e\omega_0 \mathscr{E}, \qquad \text{(B2)}$$

where ω is the Schubweg or average range of the electrons, ω_0 is the Schubweg per unit field, $\mathscr{E}$ is the electric field strength between the plates, and L is the sample thickness Following an ESA

transition which photoionizes a cerium ion, the electron can either remain at the cerium site or migrate away to form a dipole and the quantum efficiency for the production of dipoles is η.

The dependence of the ESA coefficient on pump-to-probe delay is identical to the fluorescence lifetime of the lowest 5d level of the Ce^{3+} ions. This then identifies the lowest 5d level as the initial state for the ESA transition. The spectral dependence of the ESA is displayed in Fig. B1. The ESA spectrum is seen to rise monotonically from 600 to 680 nm as has been previously measured,[13-15] peaks at approximately 700 nm, and then falls steadily with increasing wavelength. Equation (B1) can be used to determine the ESA cross-section. At the 700 nm peak, the ESA cross section is $\sigma^*=(1.0\pm0.3)\times10^{-17}$ cm^2 for 500 nm pumping. The large value of the cross-section indicates that the ESA does not terminate on a crystal field split level of the 5d manifold. The shape of the ESA spectrum is striking similar to other photoionization spectra in semiconductors and alkali halides. Measurements of σ^* using a 308 nm excitation pulse indicate that the pumping quantum efficiency β at this wavelength is 0.17 instead of 1.0. This reduced value of β for the UV pumping would suggest that energy states in addition to the lowest 5d state of the Ce^{3+} ions are being excited by these shorter pump wavelengths.

The kinetics of the 5d population following a pump-probe pulse sequence are shown in Fig. B2. Here a strong probe pulse is used to partially saturate the ESA. The depopulation of the 5d state is evident from the sudden drop in the 5d$\rightarrow$4f fluorescence concurrent with the arrival of the probe pulse.

The photoconductivity measurments indicate that significant photoionization occurs when a 460 nm pulse is temporally followed by a 700 nm pulse. 460 nm is at the peak of the lowest 5d absorption and the 700 nm corresponds to the peak of the ESA spectrum. This photocurrent, which is observed when both beams impinge upon the sample, is due to the two–step photoionization of the cerium ions. Continued illumination of the sample in an electric field produced a significant permanent dipole moment. Thermal annealing of the sample quenched this moment by recombining the trapped electrons with the cerium hole centers.

An extrapolation on the low energy side of the ESA spectrum of Fig. B1 predicts that the conduction band edge lies about 10000 cm^{-1} above the relaxed lowest 5d level. If we add this energy to the 20440 cm^{-1} between the 4f ground state and the relaxed lowest 5d level, we would predict a photoionization threshold for transitions originating on the 4f state of about 30440 cm^{-1}. This value is in excellent agreement with the ground state photoconductivity results[19] of a 30650 cm^{-1} (3.8 eV) threshold. This relationship between the energies of the cerium levels and the band states of the YAG host is illustrated in Fig. B3. The valence band to conduction band gap is 50000 cm^{-1}. The positions of the bottom of the two lowest 5d levels relative to the 4f ($^2F_{5/2}$) state are fixed from the measured no–phonon transition energies. The conduction band edge is seen to overlap the position of the second 5d level. Thus the wave functions describing the states at energies higher than the conduction band edge involve a superposition of delocalized Bloch states and the more localized d–like orbitals of the cerium ion. The matrix elements describing the transitions originating from the 4f level to this region are sensitive to both the 5d and plane wave components. This is reflected by the 4f→5d resonances superimposed on the rising 4f→conduction band absorption in the ground state absorption spectrum. However, the ESA transition which originates from the lowest 5d orbital, is much less sensitive to these higher d–like states and the transition moment will be dominated by the dipole matrix elements between the lowest 5d orbital and the delocalized Bloch states.

Since the second 5d state overlaps the onset of the conduction band, optical pumping into this region can result in both the direct excitation of the cerium ions as well as the population of the electron trapping sites via the conduction band. Thus the ESA due to optically excited cerium ions would be observed simultaneously with other absorption processes involving these trap sites. This model for the multicomponent ESA is consistent with our measurements of the room temperature ESA kinetics for 308 nm pumping as well as those by Jacobs *et al.*[13] for 350 nm pumping and Miniscalco[14] for 337 nm pumping. Since the lifetime of these transient color centers is governed by thermal excitation back into the conduction band, the decay rate of the absorption mediated by these color centers should be temperature dependent. The measurements

by Owen *et al.*[15] at 77 K with 337 nm pumping of transient absorptions having 165 s and 11 min decay components is indicative of this temperature dependent relaxation. Our observation of a 60% reduction in the time–integrated cerium fluorescence in the presence of a strong 680 nm probe pulse points to a competitive relaxation channel of the color centers which does not repopulate the cerium sites. This alternate relaxation mechanism is also expected to be temperature dependent.

The 337 nm and 350 nm pump wavelengths mentioned above are both below the photoionization threshold at 326 nm determined by Pedrini[19] and thus should not directly photoionize the cerium ions. Nevertheless, intense laser pumping into band–tail states can result in an appreciable number of photoionized cerium ions. The importance of these band tail states is also evident from our observation of a significant photocurrent when the Ce:YAG sample is illuminated with the 3rd harmonic of a Nd:YAG laser at 355 nm. Since the photoresponse was a linear function of the 355 nm photon flux, the photoconductivity is due to a single photon transition at this wavelength.

These results may have important implications for other potential solid state laser materials. Even when the higher lying energy states of the dopant ion are absent or have low transition cross sections from the laser level, photoionization transitions to the host conduction band may still degrade or inhibit laser operation in the material. The strength and spectral position of these ESA transitions to the conduction band can not be determined directly from ground state absorption measurements.

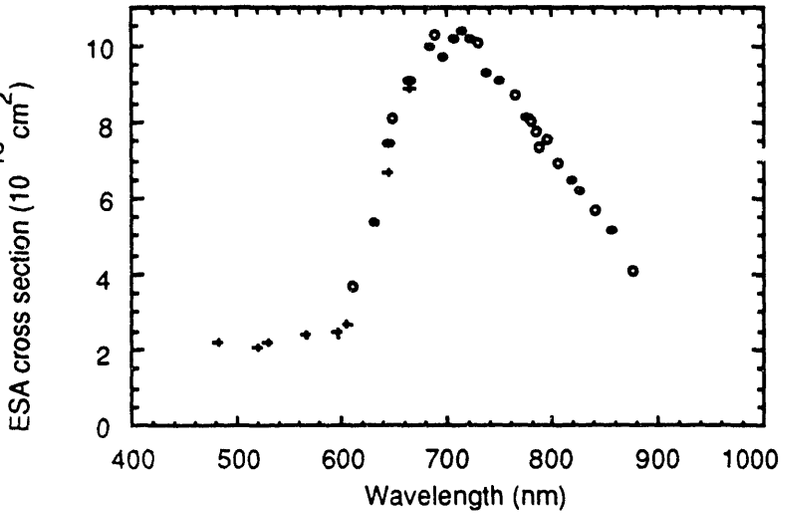

Figure. B1. Wavelength dependence of the excited state cross section σ*. The circles are the values measured in this work, the crosses are the scaled values from Miniscalco *et al.*

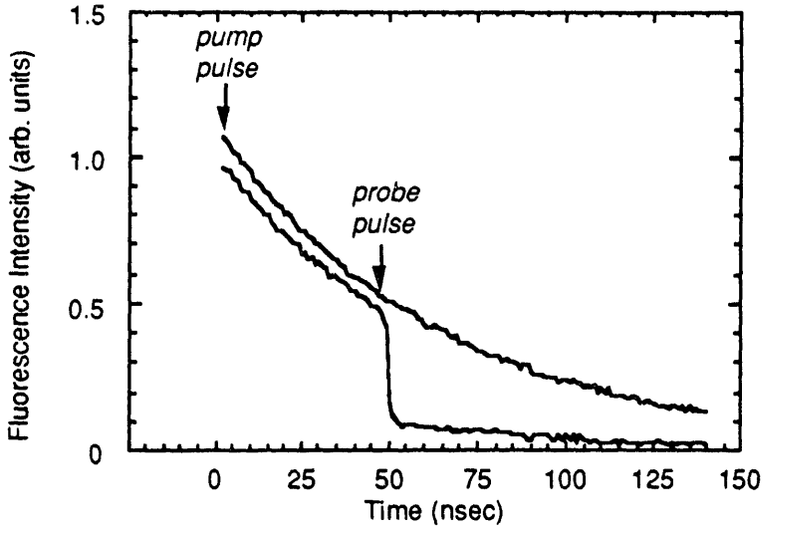

Figure. B2. Decay of the lowest 5d state in Ce^{3+}:YAG. The upper trace shows the decay following pulsed excitation at 500 nm. The lower trace shows the depopulation of the 5d state due to a strong 700 nm probe pulse at a 50 ns time delay.

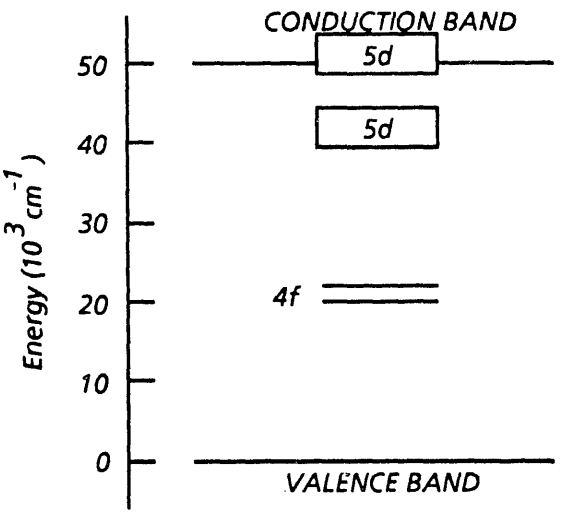

Figure. B3. Positions of the Ce^{3+} states relative to the conduction and valence bands of the YAG host.

C. Excited state photoionization of Ce^{3+} ions in $Ce^{3+}:CaF_2$

*The research summarized in this section has been published in 3 journal articles ["Laser Induced Defect Centers in $Ce^{3+}:CaF_2$," G.J. Pogatshnik, S.K. Gayen and D.S. Hamilton, J. Lumin. **31/32**, 251 (1984), "Excited State Photoionization of Ce^{3+} ions in $Ce^{3+}:CaF_2$," G.J. Pogatshnik and D.S. Hamilton, Phys. Rev. B **36**, 8251 (1987), "Rate Equation Description of Multi-photon Creation of Color Centers and Simultaneous One-photon Annihilation," G.J. Pogatshnik and D.S. Hamilton, J. Lumin. **38**, 201 (1987)], presented at 3 conferences [International Luminescence Conference, Madison, Wisconsin, 1984, March 1986 Meeting of the American Physical Society, 6th International Conference on Dynamical Processes in Excited States of Solids, Tsukuba Japan, 1987] and formed part of the Ph.D. thesis of Gerald J. Pogatshnik.*

The spectrally broad vibronic emission bands in impurity doped solids serves as the basis for wavelength-tunable laser operation in these materials. But because of the broad emission and absorption bands, these materials are susceptible to excited-state absorption (ESA) which can significantly reduce the performance characteristics of the laser material. We have observed a strong ESA in $Ce^{3+}:CaF_2$ at the optical pumping wavelengths which lie in the near ultraviolet.[20-23] It is a two-step process, where the first photon absorbed promotes an electron from the 4f ground state to the lowest 5d state of the trivalent cerium ion. Within the lifetime of this excited 5d state, a second photon is absorbed which then photoionizes the ion by promoting that electron to the conduction band. The free electron subsequently traps out at an electron acceptor site forming a stable color center. These color centers are absorptive at the wavelengths for stimulated emission of the trivalent cerium ions, and hence they serve as a quenching mechanism for laser gain in this crystal. The color centers produced are photochromic in that they can be optically bleached.

We have pursued the understanding of this two–step photoionization and color center formation process in some detail, motivated by the facts: (a) that similar processes may occur in other lanthanide or transition metal ion doped solid state laser materials which would operate in the deep blue or near ultraviolet, (b) that the UV induced discoloration is a prototypical laser damage process for which an impurity ion serves as a nucleation site, (c) that photochromic materials have significant potential in optical storage technologies, and (d) that $Ce^{3+}:CaF_2$ is a well studied

material and thus much of the background information concerning its optical properties is already in hand. We will demonstrate that the properties of these laser induced color centers can be explained by a model based on the excited-state photoionization (ESPI) of the cerium ions.

When cerium is incorporated into CaF_2 as an impurity ion, it enters in a trivalent state and substitutes for a calcium ion. The substitution of a Ce^{3+} ion for a Ca^{2+} ion requires the presence of an additional charge compensator to maintain the overall charge neutrality of the crystal. The dominant charge compensation scheme is an additional F^- ion located in the nearest body center cube position to the cerium impurity, so that the symmetry of the cerium ion is C_{4v}. In addition to the C_{4v} sites, there are also a few cerium ion sites which maintain their cubic symmetry. These O_h symmetry sites occur when the F^- charge compensator is located further away from the trivalent cerium ion. The presence of cerium ions at sites of cubic symmetry is of great importance in this investigation, since cerium ions at these sites have previously been shown to be relatively stable in a divalent, as well as trivalent state.[24,25] Thus, the trivalent ions at O_h sites can act as electron traps in the crystal.

The lowest $4f \rightarrow 5d$ absorption band of the Ce^{3+} ions is resonant with the 308 nm output of a XeCl excimer laser. Illumination of the sample at this wavelength, using a Quanta Ray EXC-1 excimer laser, produces long-lived color centers in the material. The presence of these centers can be observed visually, with the sample changing from its original transparent state to a reddish-brown color. The mechanism responsible for this coloration is directly linked to the excitation of the cerium ions. Comparable flux illumination using the 337 nm output of a nitrogen laser, or the 355 nm output of the third harmonic of a Nd:YAG laser, both of which are non-resonant with the cerium absorption bands, produces no coloration of the crystal. Similarly, no coloration of undoped CaF_2 is observed after exposure to the 308 nm laser light. Thus the coloration process must involve the cerium ion in the excited 5d level.

The centers that are responsible for this coloration are photochromic, in that the crystal can reversibly change color under optical illumination. That is, the Ce^{3+}:CaF_2 sample can be bleached back to the original transparent state by illumination of the sample at wavelengths which are

absorbed by the color centers. The bleaching process presumably takes place by a one–step photoionization transition on these centers. The optical absorption spectrum of the color centers produced by the UV laser irradiation at 308 nm is identical to the optical properties of divalent cerium ions at O_h sites in CaF_2. The presence of Ce^{2+} in CaF_2 has been previously observed in both γ-irradiated crystals[24] and crystals treated by additive coloration.[25]

The photoionization of the Ce^{3+} ion in CaF_2 does not occur in a one photon absorption process. The absorption spectrum for Ce^{3+}:CaF_2 shows that the absorption band for the lowest 4f→5d transition lies well below the conduction band transition. Therefore, one expects that the absorption of a 308 nm photon results in a purely localized transition at the cerium site. Nevertheless, intense laser pumping of the Ce^{3+}:CaF_2 sample at 308 nm does lead to a strong photoconductivity signal.[22] This suggests that a multiphoton process involving the Ce^{3+} ions is required for the photoionization of the trivalent cerium ions and the subsequent production of the divalent cerium centers.

To determine in more detail the processes responsible for coloration of the crystal following UV excitation, we have measured the absorption produced by the presence of Ce^{2+} ions as a function of laser intensity and elapsed exposure time. The intensity of the transmitted probe beam was measured at a fixed 308 nm laser flux for a series of incident laser pulses. The resulting change in the optical absorption produced by the creation of divalent cerium centers was then calculated. Typical data curves for the UV laser induced absorption as a function of the number of laser pulses for a series of different incident laser intensities is illustrated in Fig. C1. At a given laser intensity, the absorption of the 520 nm probe beam due to the Ce^{2+} centers increases for the first few laser pulses and then eventually reaches a steady state level. For low laser intensities the value of the steady state absorption coefficient is almost linearly dependent on the incident laser intensity. As the intensity of the 308 nm laser increases, the value of the steady state absorption coefficient begins to saturate, and becomes fixed at a value which is independent of laser intensity.

This saturation of the steady state density of divalent cerium ions at high laser intensities indicates that there is an upper bound on the number of these centers which can be produced. The

magnitude of the steady state absorption coefficient depends on the laser intensity and the cerium concentration in the sample, but is independent of the initial concentration of Ce^{2+} ions. For example, illuminating the sample at high laser intensities produces a relatively dark crystal. If the intensity of the laser is now decreased and the illumination continued, the optical density of the sample will be reduced until it again reaches a steady state value. The density of Ce^{2+} centers in this process is the same as one would have obtained through illumination of an originally transparent sample at the lower laser intensity. This behavior indicates the non-linear nature of this process. If both the creation rate and bleaching rate for producing the divalent cerium centers were linearly dependent on the incident laser intensity, additional exposure to the reduced intensity laser light could not account for the decrease in the steady state optical absorption of the sample.

The steady state absorption in these samples reflects an equilibrium between the creation of the divalent cerium centers and their optical bleaching at a particular value of the laser intensity. To determine how the creation of the centers depends on the incident laser intensity, we have examined the slope of the absorption curves of Fig. C1 in the limit as the number of laser pulse exposures goes to zero. The extrapolation to the initial slope should be an accurate reflection of the creation process since the competing bleaching term will depend on the initial concentration of Ce^{2+} centers. Initially, this concentration is approximately zero, so that the bleaching effects can be ignored. Figure C2 shows the initial slope of the induced absorption from this analysis as a function of laser intensity. At low laser intensities, the log-log plot is nearly linear with a slope of two. This indicates that the creation process for the divalent cerium centers depends on the square of the 308 nm intensity and thus two photons are required to photoionize the Ce^{3+} ions. At higher intensities, the dependence of the initial slope on the laser intensity begins to roll off and eventually becomes quasi-linear. For sufficiently high laser flux, bleaching and saturation effects cannot be ignored even during the first laser pulse.

The appearance of divalent cerium is initiated through the photoionization of Ce^{3+} ions, which are predominantly at C_{4v} sites in the CaF_2 crystal. This photoionization process occurs by an ESA transition from the excited 5d state of the Ce^{3+} ion. Trivalent cerium ions at cubic sites in

the crystal act as trap sites for these electrons. Since the charge compensator at these O_h symmetry sites is somewhat removed from the cerium impurity, the Ce^{3+} ions at these sites will have a net positive local charge associated with their lattice position. The Coulombic field produced by these ions provides a net attractive potential for electrons in the conduction band which causes them to trap at these sites. This trapping results in the formation of divalent cerium ions at the cubic sites and accounts for the coloration of the crystal. Subsequent illumination into the Ce^{2+} absorption bands ionizes these centers, and returns some of the electrons to the originally ionized sites. This restores the valence state of all the cerium ions to trivalent and accounts for the photochromic behavior of this material. The flux dependence of the steady state absorption coefficient due to the divalent cerium centers reflects the competition between the creation and bleaching of these centers. Since the bleaching term is linear in intensity and the creation term is non-linear, the equilibrium value of the divalent cerium ion density will be dependent on the incident laser intensity. We have been able to sucessfully model the intensity and exposure time dependance of the Ce^{2+} color center density by a rate equation which incorporates a creation term which is quadratic in the laser intensity and a bleaching term which is linear in the laser intensity.[21,23] The rate equations implicitly include the finite number of electron acceptor sites. Solutions to the rate equations correclty descibe the initial rate of production of color center which is quadratic in the intensity, and the high and low intensity limits of the steady-state color center density.

Figure C3 illustrates the essential features of the model for ESPI in Ce^{3+}:CaF_2. Laser excitation of the lowest 4f→5d transition results in the photoionization of the Ce^{3+} ion through the 5d state. The electron is promoted to the CaF_2 conduction band where it has sufficient mobility to be trapped at an alternate trivalent cerium site with cubic symmetry and thus form a divalent cerium center. These centers may be optically bleached by illumination into the Ce^{2+} absorption bands. This bleaching reverses the photochromic transition and returns the crystal to its original state.

In Ce^{3+}:CaF_2, the electron trap sites which are responsible for the coloration of the crystal, do not involve parasitic impurities or defects in the crystal, but result from alternate metastable valence states of the cerium ion. Our work demonstrates that systems which incorporate laser

active centers which can exist in more than one valence state, and which are subject to excited state photoionization, may experience a degradation in laser performance due to the formation of this type of color center. While the extreme stability of Ce^{2+} in CaF_2 may be exceptional, it is not unreasonable to assume that this process may occur in other laser materials as well. The photoelectrons which result from the photoionization of a laser active ion may also trap at alternate lattice sites, however the retrapping time may be on much shorter time scales than the many hours of the Ce^{3+}:CaF_2 system.

Our observation that the Ce^{3+} ions at O_h symmetry sites in CaF_2 are efficient electron acceptors suggests that other rare–earth ions in related host materials should also play a similar role. The recent measurements of photon-gated hole burning[26] in Sm^{2+}:BaClF indicate that Sm^{3+} serves as an effective electron trap site for the electrons released following the photoionization of the Sm^{2+} ions.

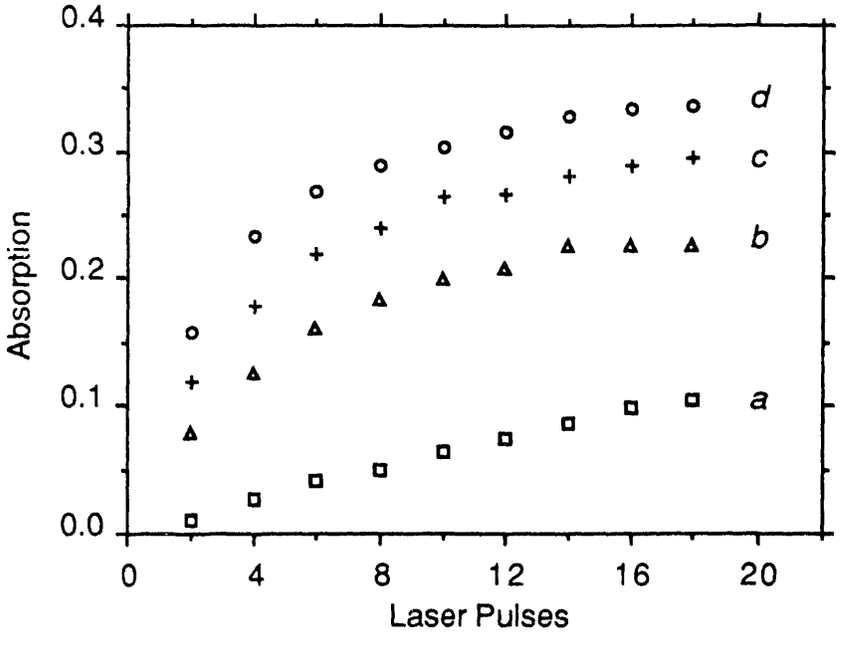

Figure C1. The absorption ($\ln I_0/I$) of a 520 nm probe beam due to the growth of the divalent cerium color centers with accumulated exposure to the pulsed 308 nm laser. The laser intensities in MW/cm^2 are: a, 10; b, 23; c, 33 and d, 44.

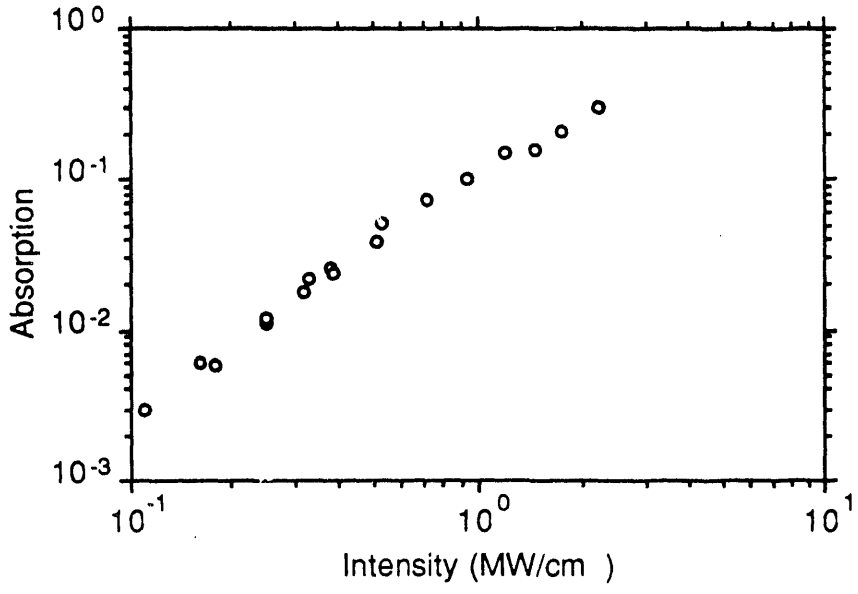

Figure C2. Initial value of the change per laser pulse in the absorption of the 520 nm probe beam. The values for the lower intensity points depend quadratically on the laser intensity, as indicated by the straight line of slope 2.

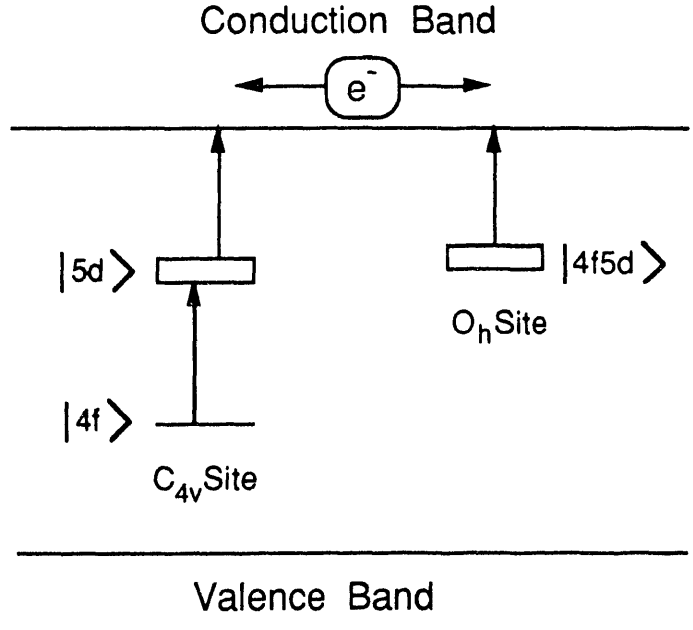

Figure C3. Proposed model for the creation and bleaching of the photochromic center in Ce^{3+}:CaF_2 based on an excited state photoionization process of the Ce^{3+} ions.

D. Optical gain and loss studies in Ce^{3+}:$LiYF_4$

*The research summarized in this section has been published in 2 journal articles, ["Optical gain and loss studies in Ce^{3+}:$YLiF_4$," Ki-Soo Lim and D.S. Hamilton, J. Opt. Soc. Am. B **6**, 1401, "UV-Induced Loss Mechanisms in a Ce^{3+}:$LiYF_4$ Laser," Ki-Soo Lim and D.S. Hamilton, J. Lumin. **40&41**, 319 (1988)], presented at 3 conferences [March 1986 Meeting of the American Physical Society, March 1987 Meeting of the American Physical Society, International Conference on Luminescence, Beijing PRC, 1987] and formed part of the Ph.D. thesis of Ki-Soo Lim.*

The broad 5d→4f vibronic emission bands of trivalent cerium doped crystals make these materials ideal candidates for tunable solid state lasers. Such cerium lasers would usually operate in the blue and near ultraviolet, at much shorter wavelengths than typical 3d systems such as Cr^{3+} and Ti^{3+}. However Ce^{3+}:$Y_3Al_5O_{12}$ shows a strong excited–state absorption[13-17] at the Ce^{3+} emission wavelengths which quenches the gain, and Ce^{3+}:CaF_2 is troubled by the formation of photochromic centers[20-23] following an excited–state absorption at the UV pump wavelengths. Both Ce^{3+}:$LiYF_4$ (YLF) and Ce^{3+}:LaF_3 do show optical gain on the 5d→4f transition,[27,28] but these two systems seem to have problems which severely limit their laser performance. The operation of the Ce^{3+}:YLF laser is hampered by several poor performance characteristics.[27] These include an early onset of saturation and rolloff in the above threshold gain and power output as well as a drop in the output for pulse repetition rates above 0.5 Hz. Our effort here is to show that an excited–state absorption of the UV pump light is responsible for a photoionization of the Ce^{3+} ions, which in turn, leads to the formation of transient and stable color centers.[29-31] The color centers have a deleterious effect on the lasing characteristics of Ce^{3+}:YLF since they absorb at the cerium emission wavelengths. The growth and relaxation of these centers impact the gain saturation and pump rate limitation of the Ce^{3+}:YLF laser.

The sample used in our measurements was an 8×8×13 mm block of $LiYF_4$ containing a nominal 1% concentration of substitutional Ce^{3+} ions and was oriented such that the c axis was

normal to the 8×8 mm face. An additional sample of undoped YLF was also studied in order to separate the effect of the cerium ions from any purely host lattice phenomena.

The cerium ions were excited by the unpolarized 308 nm output of a XeCl excimer laser having an 8 nsec pulse width. The 308 nm wavelength is in the low-energy tail of the lowest 4f→5d absorption band of the Ce^{3+} ions. At this wavelength, the optical density of the Ce^{3+}:YLF sample is 1.1 along the 13 mm path length. Three different low power cw lasers, He-Cd at 325 nm and 442 nm and a He–Ne at 633 nm were used to generate the σ polarized probe beams which interacted with the pumped volume of the sample. A coaxial pump-probe geometry was used. For the transient absorption measurements, a LeCroy 3500 transient digitizer and signal averager was used to record the transmitted probe beam intensity which was detected with a photomultiplier tube. The UV induced stable absorption spectra were measured with a Perkin Elmer Lambda 4 spectrophotometer both before and after the exposure of the sample to the 308 nm laser.

A transient reduction in the transmitted intensity of a 633 nm probe beam following a 249 nm pump pulse in Ce^{3+}:YLF was reported by Ehrlich *et al.*[27] This reduction was tentatively ascribed to thermal lensing due to the large quantum defect for the 249 nm excitation. By exciting the cerium ions at 308 nm, the thermal lensing effects should be significantly reduced due to the smaller difference between the energies of absorbed and emitted photons and the near unity quantum efficiency of fluorescence. However, our measurements indicate that even with this reduced thermal loading for a 308 nm pump pulse, a 10 mJ per pulse excitation resulted in a nearly 40% reduction in the transmitted intensity of a σ polarized 633 nm probe beam. By using a set of different diameter apertures at varying distances between the sample and the probe beam detector, we have been able to rule out thermal lensing as the cause of the reduction in the detected probe beam intensity. Since this loss was independent of the diameter and position of any aperture, there must be an absorptive process in the pumped volume of the sample.

This absorptive loss is directly related to the excitation of the cerium ions. Using an undoped YLF sample and similar 308 nm pulsed excitation, we observed no transient absorption

following the pump pulse. Thus the transient centers responsible for the absorptive loss are not created in the absence of the cerium ions. Pumping the cerium doped sample at 337 nm with a N_2 laser or at 355 nm with the third harmonic of a Nd:YAG laser, which are off–resonance with the cerium 4f→5d transition, again does not lead to any observable transient absorption. From these two observations we conclude that the creation of the color centers responsible for this transient absorption is related to the optical excitation of the cerium ions and not to any direct UV–induced color center formation in the YLF lattice.

It is also possible to rule out excited–state absorption originating on the lowest 5d state as the mechanism responsible for the transient losses. Such a process would be characterized by the 40 nsec radiative lifetime of the lowest 5d state of the cerium ions. Instead we have observed much longer recovery times for the transmitted 633 nm probe beam.[29,30]

These transient color centers absorb not only at 633 nm, but at shorter wavelengths as well. We have completed detailed measurements of the creation and relaxation characteristics of these absorption bands using laser probe wavelengths at 325 nm and 442 nm, as well as at 633 nm. The absorption band which gives rise to the 50 nsec decay component at 633 nm becomes much weaker in strength at the shorter probe wavelengths. At the He-Cd laser wavelength of 325 nm, this 50 nsec absorption component is no longer observable. On the other hand, the absorption bands with the longer lifetimes grow in strength as the probe wavelength moves to the blue. At 325 nm, a new absorption band is observed whose time decay at room temperature is approximately 30 sec.

In order to determine how these transient centers are formed, we have measured the strength of the transient absorption of a σ polarized probe beam at 633 nm as a function of the 308 nm laser intensity. As illustrated in Fig. D1, two markedly different intensity relationships are observed. The strength of the 50 ns component of the transient absorption increases quadratically with laser fluence. In contrast, the longer time components of the transient absorption at 633 nm show a near linear behavior. The quadratic dependence of the 50 ns component is characteristic of a two-photon process. As mentioned above, the transient center

responsible for the 50 ns component is not absorptive in the near-UV and thus can not be photo–bleached by the pump laser. On the other hand, the longer-lived transient centers, which show the linear intensity dependence, absorb strongly at the 308 nm laser wavelength and thus are susceptible to photo-bleaching by the 308 nm laser pulse. Significant photo-bleaching of these centers can compete with the creation mechanism and mask the expected quadratic intensity relationship.

We have been unable to detect any afterglow phosphorescence which might accompany the decay of the centers which are responsible for the transient absorption. The subsequent charge-trapping process which returns the electron to the cerium ion does not apparently leave the Ce^{3+} ion with an excited 5d electron.

Along with the transient absorptions, we have also observed temporally stable absorption bands created by the 308 nm excitation of the cerium ions. The lifetime of the stable centers is greater than a few days at room temperature. The absorption spectra due to these stable centers in Ce^{3+}:YLF following the XeCl laser irradiation is displayed in Fig. D2. The π polarized absorption band peaks near 340 nm and has an appreciable optical density at the 325 nm peak of the cerium emission band. The σ polarized absorption spectrum shows a peak at 430 nm as well as 340 nm, and this band also has some overlap with the cerium emission band. The polarized absorption bands of these UV-created color centers have also been seen in YLF following electron[32] or gamma ray[33] irradiation and have been identified as F centers. Based on the similarity of the absorption spectra, we have concluded that the stable centers in Ce^{3+}:YLF created by the near-UV pumping of the Ce^{3+} ions are also due to F centers.

It is also possible to optically bleach these color centers by illuminating the color centers at 308 nm, which is the same wavelength responsible for their creation. Following an exposure to a high intensity 308 nm beam, the number of centers can then be reduced by continued exposure to a lower intensity 308 nm beam. This photobleaching is more efficient at 77 K where the Ce^{3+} absorption at 308 nm is significantly less than at room temperature due to the narrowing of the $4f \rightarrow 5d$ absorption band.

The measured optical density at 325 nm due to these stable centers is a function of both the accumulated number and intensity of 308 nm laser pulses. The absorption at 325 nm is seen to grow with increasing exposure to the excimer laser and then saturate at a steady state value. The rate of growth of this optical density is also intensity dependent. The data for the initial growth rate shows a quadratic relationship indicating that a two-photon process is responsible for the initial formation of these centers. The steady state values of the optical density of these stable centers saturates with increasing laser intensity, indicating an upper bound for the number of deep trapping sites.

The transient and stable color centers play an important role in determining the Ce^{3+}:YLF laser performance characteristics since both types of centers have absorption bands which overlap the cerium emission spectrum. The influence of the longer lived transient centers can be seen from our measurement of the single-pass gain as a function of the 308 nm pump repetition rate, which is displayed in Fig. D3. The baseline value of 1.0 is the transmitted 325 nm σ polarized probe beam intensity without 308 nm pumping. If the pulse repetition rate of the excimer laser is greater than about 0.5 Hz, the quasi-steady-state density of transient color centers is large enough to result in a net loss of the transmitted 325 nm probe beam. As the repetition rate is lowered, there is more and more time for the transient color centers to relax before the arrival of the next pump pulse and thus the gain from the excited cerium ions becomes larger than the losses from the color centers. Thus the gain measured after any particular pump pulse is reduced by the loss due to steady state density of the more stable centers, the loss due to the density of transient centers created by that pump pulse, and the density of transient centers which remain from all of the previous pump pulses. Only the last mechanism is dependant on the pulse repetition rate. We estimate from the stimulated emission cross section[27] at 325 nm, that the single pass gain in the absence of these color center losses would be about 1.7 for the 5 mJ/7 mm^2 excitation pulse.

The quadratic dependance of the initial growth of the stable centers and the strength of the shortest time component transient absorption on the laser intensity indicate that two 308 nm

photons are required to create both types of color centers. With a band gap in YLF corresponding to approximately 120 nm, the fact that two photons at 308 nm can photoionize the Ce^{3+} ion suggests that their is a significant energy gap between the top of the valence band and the 4f level of the Ce^{3+} ion. Since the centers are formed only at wavelengths resonant with the 4f→5d absorption of the Ce^{3+} ions, this two photon process involves an excited–state absorption (ESA) on the Ce^{3+} ions. For an ESA which reaches the conduction band states of the YLF lattice, the electron will have sufficient mobility to find and become trapped at alternate lattice sites. Different charge-trapping sites will result in different binding energies and energy level structures for the color center. In addition to creating the color centers, the 308 nm laser pulse can also annihilate them by a photo-bleaching process. Thus the description for the growth, intensity dependance and saturation characteristics of the color center population must incorporate both a quadratic creation term and a simultaneous photobleaching term.

In order to fully understand the growth, intensity dependance and saturation characteristics of the color center population, we have developed rate equations appropriate for a time series of finite duration laser pulses. The rate equation is integrated over the j^{th} laser pulse and then the solution is allowed to relax until the next (j+1) laser pulse occurs at a time delay T. This procedure then gives a series which can be summed for any arbitrary number of pulses N and time delay T. The solutions thus developed were successfully applied to the growth and saturation characteristics of both the stable and transient color centers.

The characteristics of the color center formation described here will have an important effect on the the lasing properties of flash-lamp pumped Ce^{3+}:YLF and implications for other materials as well. If the spectral content of the flash-lamp is broader than or is not matched to the the Ce^{3+} absorption bands, then the photons outside the Ce^{3+} bands will not contribute to the excitation of the cerium ions but can promote excited–state absorption processes which may photoionize the cerium ions and lead to color center formation. These spectrally non–matched photons thus do not just lower the wall–plug efficiency of the laser, but serve to increase

threshold and saturation problems as well. Such considerations may be responsible for the inability to achieve a net stimulated gain in flash-lamp pumped Ce^{3+}:YLF crystals.[34]

We have demonstrated that the optical pumping of Ce^{3+}:YLF in the near ultraviolet leads to the formation of both transient and stable color centers. These centers clearly play an important role in determining the device characteristics of a Ce^{3+}:YLF laser. The relaxation of the transient centers governs the repetition rate limitation. Both the stable and transient centers mediate the gain saturation and slope efficiency as well as the lasing threshold. The photoionization of the Ce^{3+} ion requires two photons at 308 nm to reach the conduction band of the host crystal. If the color center produced following this photoionization is also absorptive at the 308 nm pump wavelength, then the competition between the photobleaching process and the creation mechanism can mask the simple quadratic intensity dependance. If the more permanent color centers involve fluorine vacancies, it may be possible to reduce the absorptive losses by improved crystal growth and treatment. For transient centers related to the presence of the cerium ions themselves, there is much less of an opportunity to reduce the their deleterious role.

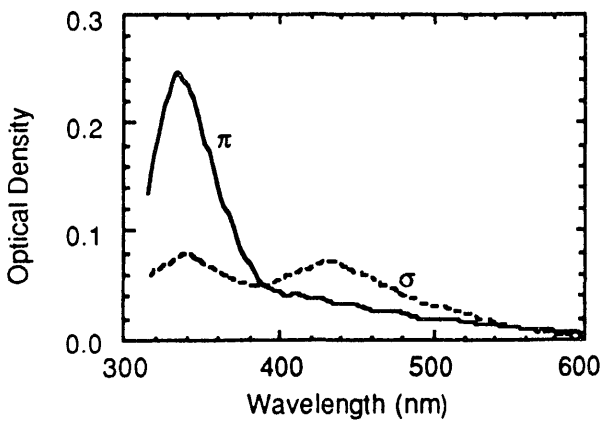

Figure D1. Polarized absorption spectra of the Ce:YLF sample following irradiation at 27 MW/cm^2 for about 2000 laser pulses at room temperature.

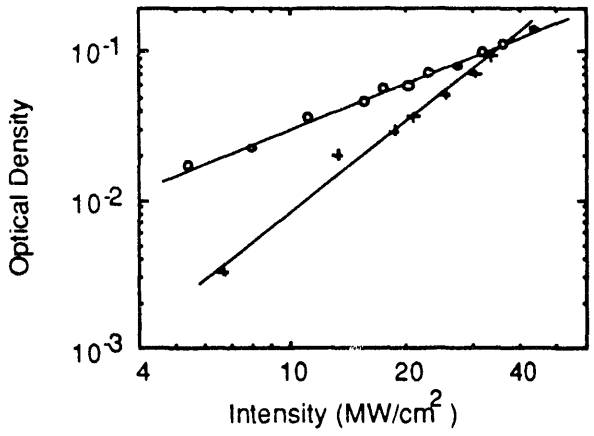

Figure D2. The transient absorption at 633 nm as a function of the XeCl laser intensity. The circles (o) represent the absorption at 50 μs after the laser pulse and are shown along with a straight line whose slope is 1. The absorption due to just the shortest lifetime (less than 50 ns) decay component is indicated with the plus (+) marks along with a straight line of slope 2.

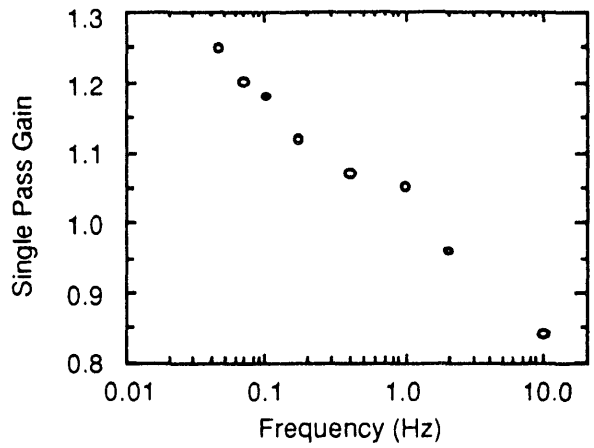

Figure D3. Single pass gain at 325 nm as a function of the repetition rate of the 308 nm pump beam.

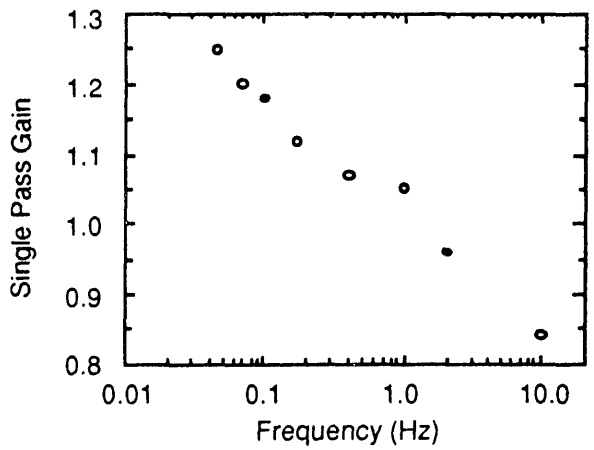

Figure D3. Single pass gain at 325 nm as a function of the repetition rate of the 308 nm pump beam.

E. Measurements of Gd→Cr energy transfer in Cr:GSGG, Cr^{3+}:GSAG and Cr^{3+}:GGG crystals

The research summarized in this section was presented at the Tunable Lasers Conference (North Falmouth MA, 1989) and the conference proceedings are being published by the Optical Society of America.

There continues to be active interest in rare-earth and transition-metal doped GSGG [$Gd_3Sc_2(GaO_4)_3$] for high power and tunable laser applications.[35]. This is specially true for Cr:GSGG and Nd:Cr:GSGG, where in the second material, the Cr→Nd energy transfer is an efficient mechanism to pump the Nd ions. Recent laser-induced grating experiments have been used to study Cr→Cr energy transfer in chromium doped garnets.[36] Here we report on the observation of a rapid Gd^{3+}→Cr^{3+} energy transfer process in Cr^{3+}:GSGG and in the two related chromium-doped gadolinium garnets Cr:GSAG [$Gd_3Sc_2(AlO_4)_3$] and Cr:GGG [$Gd_3Ga_2(GaO_4)_3$]. The large energy of the Gd^{3+} exciton (≈30,000 cm^{-1}) has implications for photoionization and color center formation in these materials. We have also observed nonexponential and wavelength dependent decay dynamics for the Cr^{3+} ion in GSAG and GGG. These results are interpreted in terms of an inhomogeneous site distribution for the Cr^{3+} ions.

The experimental apparatus employed to investigate the Gd^{3+}→Cr^{3+} energy transfer uses a dye laser pumped by the second harmonic of a Q-switched Nd:YAG laser. The dye laser output is used to directly pump the Cr^{3+} absorption bands or can be frequency doubled to reach the the 300 nm wavelengths appropriate for the Gd^{3+} absorption. The LeCroy #3500 transient digitizer and signal averager is used to record the Cr^{3+} fluorescence with a 10 nsec time resolution. The absorption spectra were taken with a Perkin-Elmer Lambda 4C spectrophotometer and the excitation spectra were recorded with a Spex fluorolog spectrofluorimeter. Measurements were performed at both room temperature (300K) and 77 K. The Cr:GSGG and Cr:GSAG samples where grown by the Czochralski technique at Union

Carbide and had a 1.0 at.% Cr^{3+} doping. The Cr:GGG samples were grown by Material Progress and also had a nominal 1 at.% Cr^{3+} concentration.

The absorption spectra of Cr:GSGG is dominated by the broad $^4A2g \rightarrow {}^4T_{2g}$ and $^4A2g \rightarrow {}^4T1g(a)$ transitions of the Cr^{3+} ion. In the gadolinium garnets there are also narrow absorption bands near 310 nm and 280 nm as shown in Fig. F1. These absorption bands are transitions from the $^8S_{7/2}$ ground state of the Gd^{3+} ion to the ^6P and ^6I manifolds of excited states. The three peaks at 313, 307 and 302 nm correspond to the $^8S_{7/2} \rightarrow {}^6P_{7/2}$, $^8S_{7/2} \rightarrow {}^6P_{5/2}$, and $^8S_{7/2} \rightarrow {}^6P_{3/2}$ transitions of the Gd^{3+} ion. Higher resolution absorption spectra show the Stark splitting in the various manifolds. The absorption spectra in Cr:GSAG and Cr:GGG also show these same absorption bands with only a weak dependence of the Gd^{3+} transition wavelengths on crystal composition.

We have measured the excitation spectra of these Cr^{3+} doped garnets by monitoring the Cr^{3+} $^4T2g \rightarrow {}^4A2g$ emission intensity as the wavelength of the exciting light was varied in the region of the Gd^{3+} absorption bands. The room temperature excitation spectrum of Cr:GSGG is displayed in Fig. F2. The three peaks between 300 and 315 nm again correspond to the $^8S_{7/2} \rightarrow {}^6P_{7/2}$, $^8S_{7/2} \rightarrow {}^6P_{5/2}$, and $^8S_{7/2} \rightarrow {}^6P_{3/2}$ transitions of the Gd^{3+} ion. The correlation between these peaks in the excitation spectra with those in the absorption spectra due to Gd^{3+} indicates significant $Gd^{3+} \rightarrow Cr^{3+}$ energy transfer is occurring. Similar Gd^{3+} absorption peaks appear in the Cr3+ excitation spectra in GSAG and GGG. The fluorescence spectra obtained by exciting the Gd^{3+} ions is the same as that produced following the Cr^{3+} excitation except for a very weak and broad band at 800 nm observed in the GGG sample. We have attributed this extra emission band to trace Fe^{3+} impurities which are excited by a $Gd^{3+} \rightarrow Fe^{3+}$ energy transfer.

We have also measured the time resolved decay dynamics of the Cr^{3+} ion following excitation into either the Cr^{3+} or Gd^{3+} absorption bands. A tunable dye laser with an optional frequency doubler was used as the excitation source. The dye laser had an nominally 10 nsec duration pulse. Typical chromium fluorescence decay curves following ^4T2g pumping in Cr:GSGG with the dye laser is shown in Fig. F3. The decay for Cr:GSGG is exponential over

two decades and the lifetime at 300K was determined to be 114±2 μs. An identical decay lifetime is obtained for pumping the $^4T_{1g}$ Cr^{3+} transitions. At a sample temperature of 77 K, the lifetime increases to a value of 187±2μs. The decay curve for Cr:GGG has a nonexponential time dependence. Moreover, the detailed shape of the decay curve changes with both excitation and emission wavelength. This markedly non-exponential decay in Cr:GGG has also been observed by Powell[36] at low temperatures and was attributed to the statistical occupancy of the next nearest neighbor sites with Gd^{3+} instead of Ga^{3+}. Thus the nonexponential nature of the decay is arises from a superposition of Cr^{3+} ions with different local crystal field environments. Our measurements indicate that this nonexponential behavior persists even up to 300 K. The decay dynamics for Cr:GSAG are much less non-exponential than those of Cr:GGG. The Cr^{3+} lifetimes are summarized in table I.

TABLE I. Summary of the mean Cr^{3+} fluorescence decay times (T_d). A * indicates that the process is not characterized by a single parameter.

host	T_d(300K)	T_d(77)
GSGG	114 μs	187 μs
GSAG	155 μs	260 μs*
GGG	185 μs*	1200 μs*

The short time dynamics of the Cr^{3+} emission at 300 K for 312 nm excitation into the lowest Gd^{3+} absorption band is displayed in Fig. E4. The rise time of the Cr^{3+} fluorescence following excitation of the Gd^{3+} ions is a measure of the $Gd^{3+}\rightarrow Cr^{3+}$ energy transfer rate. Assuming a single transfer time of T_t, the initial growth has been fit to the expression

$$I(t) = I_\infty[1-\exp(-t/T_t)]. \qquad (E1)$$

The resulting values of T_t are shown in table II. There is a significant host dependant variation in the transfer times and the temperature variation reflects the phonon mediated nature of the transfer process.

TABLE II. Summary of the mean $Gd^{3+} \rightarrow Cr^{3+}$ transfer times (T_t) and lattice parameters a_0. A * indicates that the process is not characterized by a single parameter.

host	T_t(300K)	T_t(77K)	a_0 (Å)
GSGG	294 ns	522 ns	12.567
GSAG	150 ns	230 ns	12.395
GGG	50 ns*	140 ns*	12.375

The description of the kinetics of an energy transfer process involves the possible migration of excitation among the donor ions (Gd^{3+}) and the ensemble average of the donor to acceptor ($Gd^{3+} \rightarrow Cr^{3+}$) transfer averaged over all possible acceptor configurations. The simplest model which gives rise to a single macroscopic transfer time is a fast-diffusion process among the donor ions followed by a single rate-limiting donor to acceptor transfer which occurs for a single donor-acceptor configuration. A fast-diffusion model for the energy migration on a Gd sublattice has been used for other Gd systems such as $LiGdF_4$ where an exchange coupling between the Gd ions leads to a fast Gd-Gd transfer.[37] Strong exchange interactions in the excited ^6P states of Gd^{3+} have been measured in $GdCl_3$ and $Gd(OH)_3$ where it results in a 2 cm^{-1} dispersion for the Gd^{3+} exciton.[38]

The cations in one octant of the garnet unit cell is illustrated in Fig. E5. The Cr^{3+} ion is located at the center octahedral site and has 6 Gd^{3+} nearest neighbors at a distance of $R = a_0/64$. In Fig. E6, the Gd→Cr transfer rate is plotted as a function of R. The transfer rate is seen to decrease with increasing Gd-Cr separation at both 300 and 77 K. A somewhat naive attempt to fit this data to a multipolar interaction of the form

$$W = f(T)\, R^{-s}, \qquad \text{(E2)}$$

where R is the Gd-Cr separation and for example s=6 for dipole-dipole coupling gives a nonsensical result of s~100. This does suggest however that the Gd-Cr coupling has a very short range dependance such as would be the case for an exchange interaction. The transfer rate for an exchange coupling would be of the form

$$W = f(T) \exp(-2R/L), \tag{E3}$$

where L is an effective average Bohr radius for the excited Gd^{3+} ion and the ground state Cr^{3+} ion. Such a short range exchange coupling is also consistent with our results on the rise-time behavior of the Cr emission. For a short range coupling between the Gd and Cr ions, one would expect the transfer to be dominated by only the nearest-neighbor Gd-Cr coupling and thus have a single dominant transfer time. A short range exchange interaction would also be sensitive to any structural disorder which would result in small changes in the Gd-Cr separation. The observation of multiple transfer rates in Cr:GGG is consistent with this model.

In addition to the many interesting spectroscopic characteristics of chromium doped garnets, there has also been reported photoconductivity measurements associated with the optical excitation of the Gd ions in Cr:GSGG[39,40] and in GGG[41]. Our results on the Gd→Cr energy transfer presented here and measurements in other Gd containing insulators do not mesh very well with a model where the direct photo-ionization of the Gd ions leads to a photoconductivity signal in these garnets. Instead we believe that the photoconductivity arises from the photoionization of lattice defects, color centers or other impurities following an energy transfer process. The Gd^{3+} exciton has sufficient energy to ionize many electron trapping sites (although presumably not Cr^{3+}) following an energy transfer process. Thus the photoionization may not be taking place on the Gd ion, but rather at other sites in the crystal. Such multistep photoionization might be significant in describing color center formation and solarization processes in these garnet laser hosts.

In situations where the exciting light is not in the near-UV, it is still possible to efficiently pump the 4f→4f transitions of the Gd^{3+} ion by intense visible radiation via a two-photon

absorption process. Such two-photon transitions have been observed for the Gd^{3+} ions in $Gd:LaF_3$ for the $^8S \rightarrow {}^6P$ transitions[7] as well as for the $^8S \rightarrow {}^6I$ and $^8S \rightarrow {}^6D$ transitions.[9] Although the $4f \rightarrow 4f$ transitions of Gd^{3+} are first-order dipole forbidden for a one-photon process, this selection rule is lifted for a two-photon process.

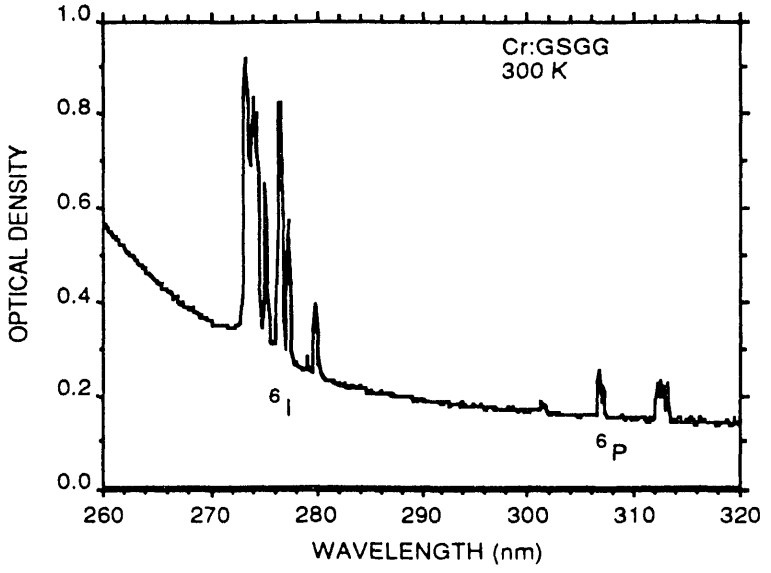

Figure E1. Absorption spectra from 260 to 320 nm of Cr:GSGG at 300 K. The sample thickness is 0.2 mm. The spectra is not corrected for reflectivity losses.

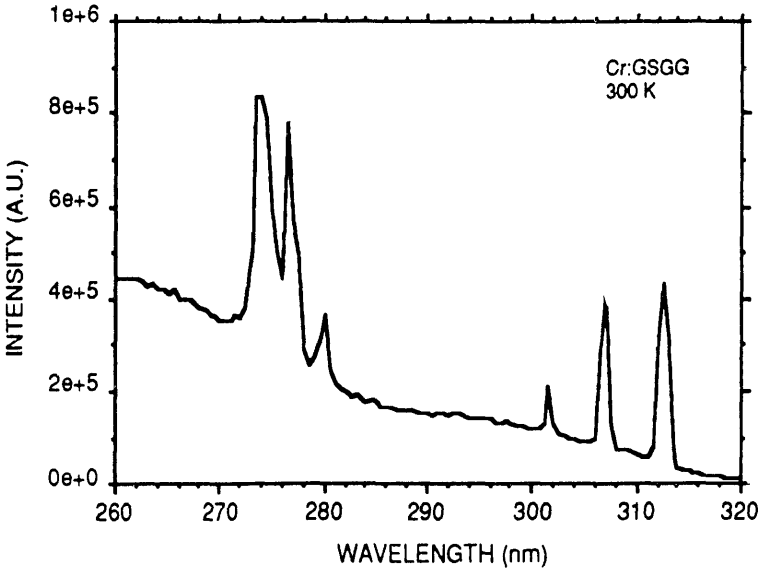

Figure E2. Excitation spectrum of Cr:GSGG at 300 K. The Cr^{3+} emission was detected at 695 nm.

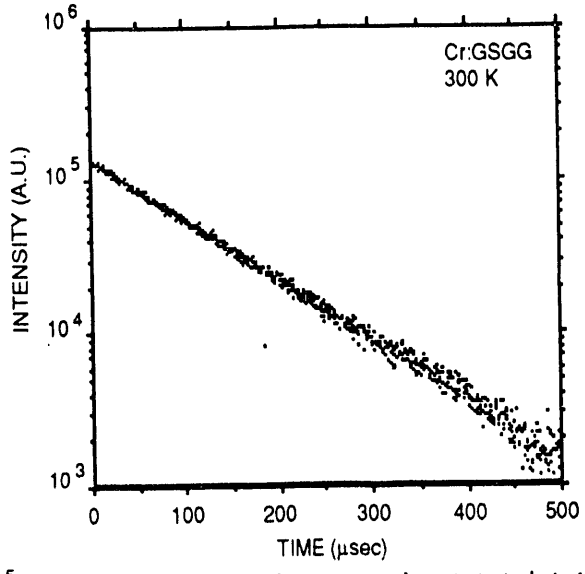

Figure E3. The decay of the Cr^{3+} emission in Cr:GSGG at 300 K. The pumping wavelength was 460 nm and the fluorescence was monitored at 750 nm.

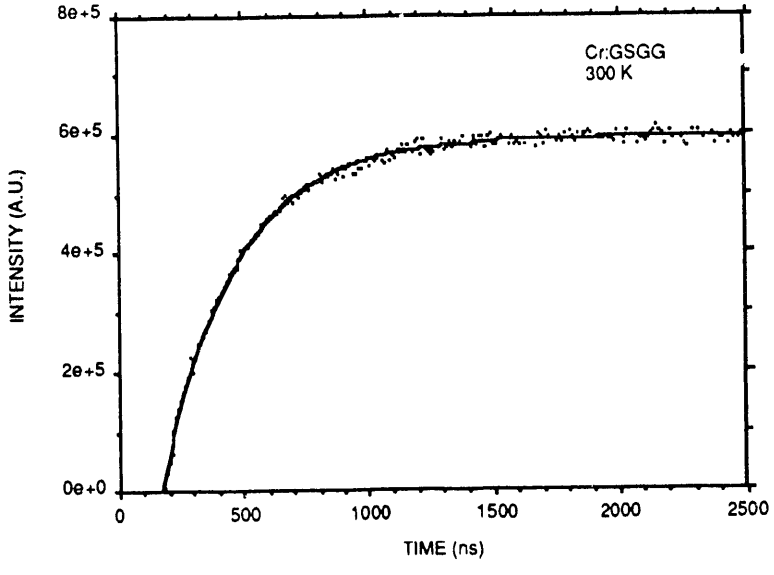

Figure E4. Growth of the Cr^{3+} fluorescence in Cr:GSGG following pulsed excitation of the Gd^{3+} ions at 313 nm. The Cr^{3+} fluorescence was detected at 750 nm and the sample temperature was 300 K.

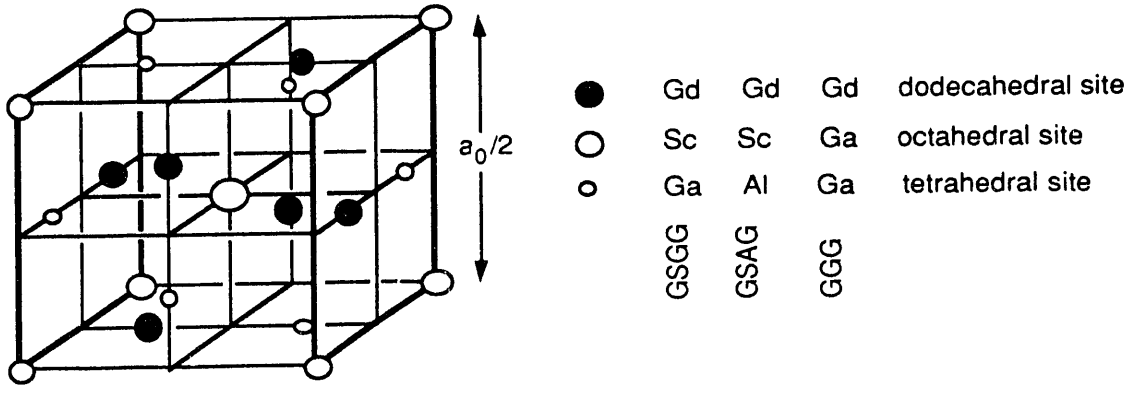

Figure E5. Location of the cations in one octant of the garnet unit cell.

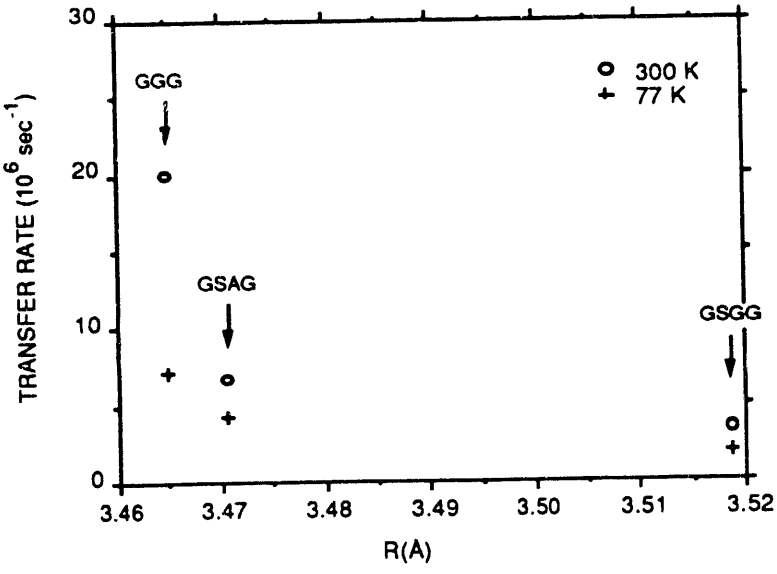

Figure E6. Transfer rate from Gd^{3+} to Cr^{3+} as a function of the Gd-Cr separation.

F. Nonradiative relaxation measurements in Ce^{3+} doped crystals and glasses

The research summarized in this section iwas published as a journal article [Radiative and Nonradiative Relaxation Measurements in Ce^{3+} Doped Crystals" Li-Ji Lyu and D.S. Hamilton, J. Lumin. 48/49, 251 (1991)] presented at a conference ["Radiative and Nonradiative Relaxation Measurements in Ce^{3+} Doped Crystals" Li-Ji Lyu and D.S. Hamilton, International Conference on Luminescence, Lisbon Portugal, 1990.] and formed part of the Ph.D. thesis of Li-Ji Lyu.

The investigation of non-radiative relaxation processes in impurity doped and point-defect containing solids has been and continues to be an active area of research. This activity is driven by both the fundamental interest in ion-lattice interactions as well as the importance of non-radiative processes in device applications. Although non-radiative decay rates have been investigated intensively for color centers, transition metal ions and for the 4f→4f transitions of the lanthanides, we know of only one experimental paper[42] and one theoretical paper[43] which have considered the 5d→4f transitions in lanthanide ion doped solids. The lack of experimental work derives from the fact that the radiative decay time constant for the 5d→4f emission is typically only tens of nanoseconds and thus measurements of any accompanying non-radiative rate requires some care in experimental design and instrumentation selection. Theoretical work is also more involved since neither the weak or strong coupling limits describe these 5d→4f transitions. Our particular interest in studying the 5d→4f non-radiative rates as a function of sample temperature, sample composition and the 5d→4f energy gap stems from: (a) a desire to more fully characterize the ion-lattice interaction for the 5d electronic states, (b) the need for some phenomenological guidelines to predict trends for the non-radiative rates where the 5d→4f transitions are involved in devices such as fluorescent down-convertors, tunable lasers and phase conjugators, and (c) the fact that both the 5d→4f emission of the lanthanides and the 3d→3d emission of the transition metal ions are characterized as showing "intermediate" strength ion-lattice coupling and thus the proposed study will be complementary to those investigations in the 3d systems.

During the year we have begun the measurements of the Ce^{3+} fluorescent lifetimes for a number of Ce^{3+} doped crystals and glasses. These materials include, Ce^{3+}:CaF_2, Ce^{3+}:$LiYF_4$, Ce^{3+}:$Y_3Al_5O_{12}$, Ce^{3+}:$YAlO_3$, Ce^{3+}:YPO_4, Ce^{3+}:LaF_3, Ce^{3+}:fluoroberyllate glass, and Ce^{3+}:silicate glass. Lifetimes and absorption and fluorescence spectra are first measured at room temperature (300 K) and liquid nitrogen (77 K) temperatures. To reach the higher temperatures where the nonradiative processes become more pronounced, an oven with full optical access has been designed constructed in our machine shop.

The lifetime measurements have been completed utilizing the apparatus illustrated in Fig. F1. The excitation source for most of the measurements is a frequency doubled tunable dye laser which is pumped with the second harmonic of a Nd:YAG (Quanta-Ray DCR-1) laser. Frequency doubling crystals of KDP and BBO are used to produce wavelengths from 210 nm to 330 nm, which overlap the absorption bands of a majority of Ce^{3+} doped crystals. Lower lying absorption bands, such as those in Ce^{3+}:$YAlO_3$ are excited directly with the dye laser pumped by the third harmonic of the Nd:YAG laser. The fluorescence is collected at right angeles to the excitation beam and is focused onto the entrance slit of a 1/4 m spectrometer. The spectrometer is set to pass the fluorescence of the particular sample under study and blocks the exciting light. An Hamamatsu R928 side-window photomultiplier tube with a modified voltage divider chain is used to detect the light at the exit slit of the spectrometer. The resulting signal from the photomultiplier is then recorded by the LeCroy transient digitizer and signal averager. The LeCroy is triggered by the Q-switch timing pulse from the Nd:YAG laser and digitizes the photomultiplier signal at 10 nsec increments. The signal waveform is averaged over typically 1,000 laser pulses. The averaged waveform can then be downloaded to an Apple IIe or Macintosh SE microcomputer for analysis.

At temperatures somewhat higher than ambient, nonradiative processes become significant. For example, in Ce:YAG, lifetime shortening due to the competing nonradiative relaxation becomes pronounced at temperatures exceeding T≈500K (800 °C). To reach these high temperatures, we have designed and constructed an vacumn oven with full optical access.

The design, illustrated in Fig. F2, is a modification of that by Raptis[44] and has a maximum temperature expected to exceed 1000 °C. The furnace of Raptis was designed for Raman scattering of molten salts and was modified to accommodate crystalline and glassy samples. The oven is characterized by its small size, high thermal efficiency, and large optical solid angle of collection. Temperature measurements utilize at platinum thermocouple in contact with the sample.

Absorption and emission spectra are taken for each sample before and after the intial heating cycle. In this way we can determin any thermally induced changes in the sample due to the high temperatures in the vacumn oven. At these higher temperatures, thermally induced broadening processes can create some overlap between absorption and emission spectra in these materials. In order to avoid systematic errors due to radiative trapping, we have paid carefull attention to sample size and geometry.

The fluorescence decay for 0.5 mole % Ce^{3+}:YAG at 300 K is shown in Fig. F3. The excitation source for this measurement was a dye laser operating with Coumarin 47 at 460 nm which was pumped with the third harmonic of the Nd:YAG laser. The sample was grown by Airtron Inc. by the Czochralski technique. Using a least-squares fitting technique, the lifetime at 300 K is determined to be 63±2 nsec. This result compares well with the 62 value estimated from the work of Weber.[42] At a 77 K sample temperature, the lifetime decreases slightly to 61±1 nsec. A similar small decrease in the lifetime is evident from the lifetime vs. temperature data in Weber's paper. The nonradiative relaxation rate (W_{nr}) is plotted as a function of sample temperature in Fig. F4. Values of W_{nr} are calculated from

$$W_{nr} = 1/\tau - 1/\tau_{rad} \qquad \text{(F1)}$$

where τ is the measured lifetime and τ_{rad} is the radiative lifetime. We have assumed a temperature independent value of τ_{rad} = 63 nsec. Figure F5 shows this data fit to an Arrenious function,

$$W_{nr} = W_0 \exp(-\Delta E/kT) \qquad \text{(F2)}$$

This value of ΔE is similar to the 10,000 cm^{-1} energy gap between the lowest Ce^{3+} 5d level and the conduction band edge in $Ce^{3+}:Y_3Al_5O_{12}$ measured in our excited state absorption studies. On the basis of the similarity of the two energy gaps, we have tentatively ascribed the nonradiative rlaxation as arising from a thermal promotion of the electron from the 5d level to the conduction band. A similar model has been discussed by Payne for $Sm^{2+}:CaF_2$.

For a 0.05% $Ce^{3+}:CaF_2$ sample grown by a Brigman method at Optovac, the measured decay curve at 300 K is illustrated in Fig. F6. The dye laser used for this measurement was operated with DCM dye and then frequency doubled to 308 nm. The lifetime at 300 K is 45±2 nsec. For a 77 K sample temperature, the lifetime decreases to 39±1. Their is a significant change in the absorption and emission spectra in $Ce^{3+}:CaF_2$ following heating in vacumn to 700 C. The spectra indicate a transition from C_{4v} to C_{3v} site symetry for the Ce^{3+} ions.

The $Ce^{3+}:YLiF_4$ sample used in this study was grown by Art Linz at MIT and has an estimated 1% cerium concentration. A frequency doubled dye laser using Rhodamin 6G dye was used to excite the sample at 290 nm. The 300 K lifetime is determined to be 43±1 nsec and at 77 K the lifetime has shortened to 38±1 nsec.

The Ce^{3+} fluoroberyllate glass sample was provided to us by Dr. Marvin Weber at Lawrence Livermore Laboratory and contains 0.1 mole% CeF_3. A Rhodamin 6G dye laser was frequency doubled to 280 nm to reach the lowest 5d band of the cerium ions. The room temperature lifetime is 42±2 nsec.

In addition to studying the nonradiative relaxation in these materials, we are also investigating the radiative rates as well. Most of the samples studies so far show a 1-10% increase in the apparent radiative lifetime with increasing temperature before the nonradiative processes become important. We are attempting to develop thermally-induced mixing arguments to understand this observation. We have also considered the correlation between τ_{rad} and $\Delta E_{4f\text{-}5d}$. To the extent that the matrix element $<4f|r|5d>$ is independent of the host, the τ should scale as $(\Delta E_{4f\text{-}5d})^{-3}$. The data indicates significant correlation, with for example $Ce^{3+}:Y_3Al_5O_{12}$ having the longest radiative lifetime and the smallest value of $\Delta E_{4f\text{-}5d}$.

Table I. Summary of the lifetime measurements at 77 K and 300 K.

Sample	Excitation wavelength (nm)	Lifetime (nsec) 300K	Lifetime (nsec) 77 K
Ce^{3+}:YAG	460	63±2	61±1
Ce^{3+}:CaF_2	308	45±2	39±1
Ce^{3+}:$LiYF_4$	290	43±1	38±1

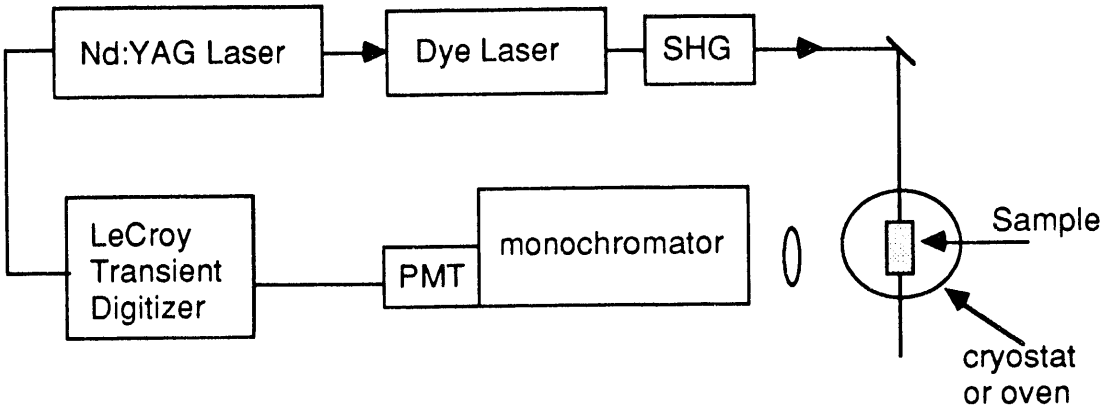

Figure F1. Apparatus used for the measurement of fluorescence lifetimes of the 5d levels of lanthanide doped crystals.

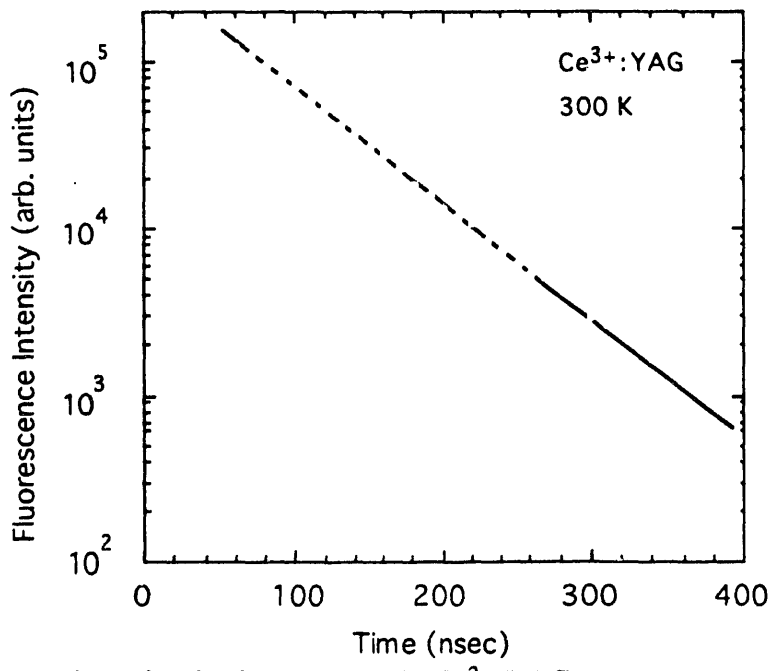

Figure F3. Decay waveform for the fluorescence in Ce^{3+}:YAG at room temperature. A least-square fit over the first two decades gives a fluorescence lifetime of 63±2 nsec.

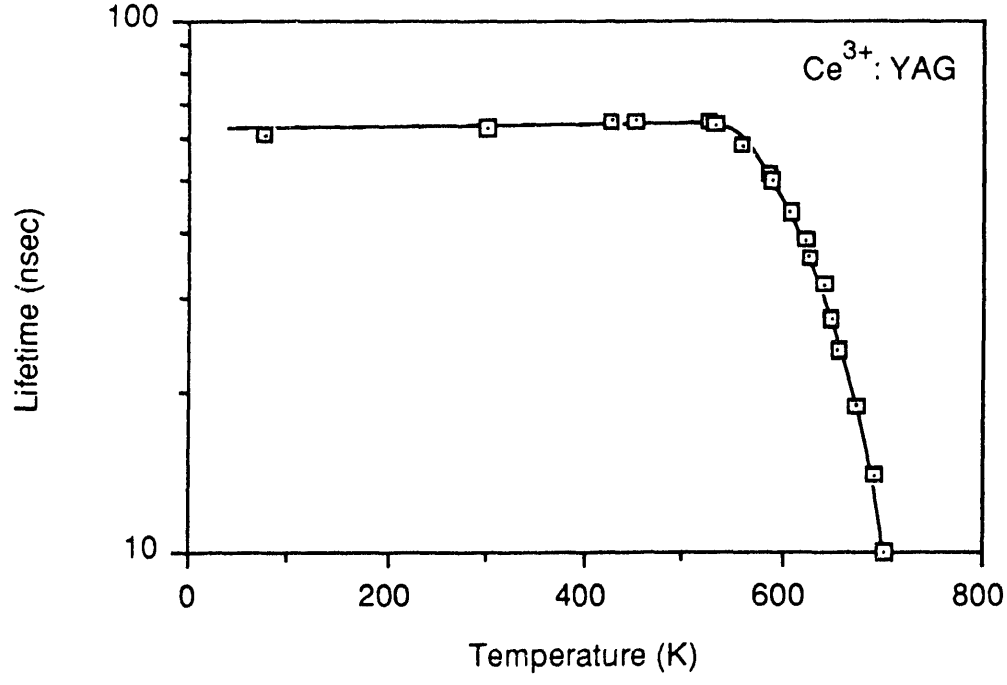

Figure F4. Temperature dependance of the fluorescence lifetime in Ce^{3+}:$Y_3Al_5O_{12}$. Significant nonradiative relaxation processes are evident above 520 K.

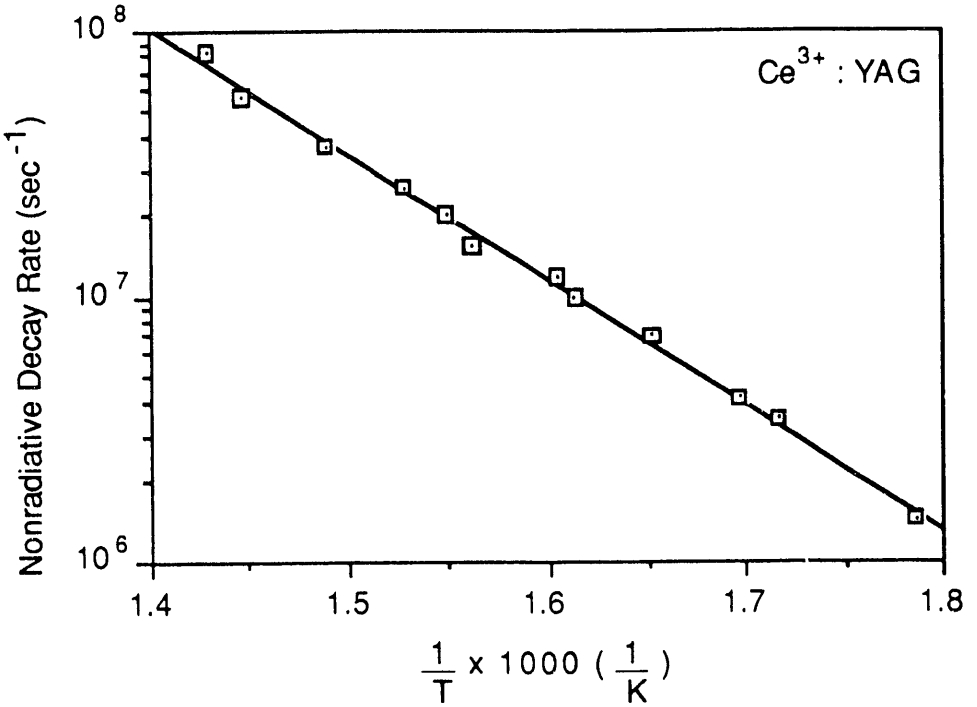

Figure F5. Nonradiative relaxation rate in $Ce^{3+}:Y_3Al_5O_{12}$ as a function of inverse temperature. The straight line fit gives an cm^{-1} activation energy.

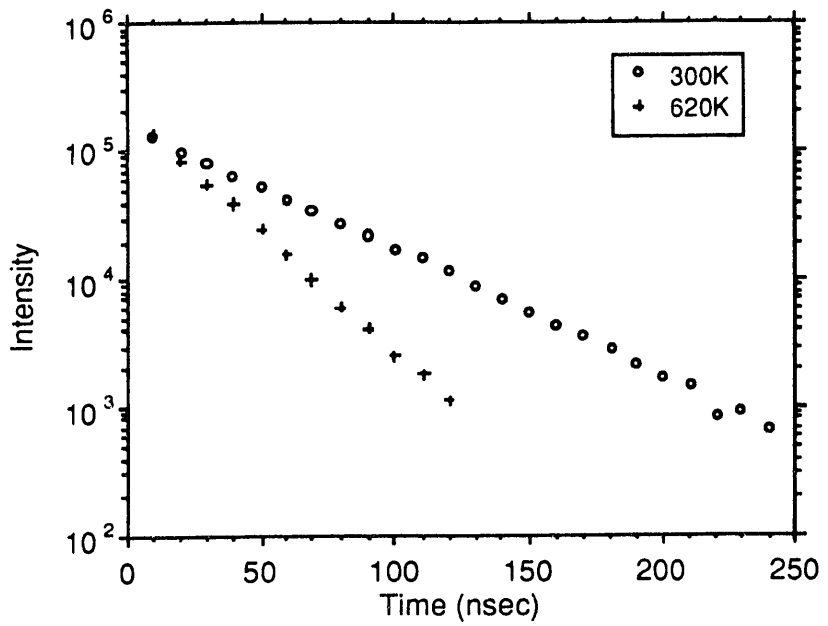

Figure F6. Decay waveform for the fluorescence in $Ce^{3+}:CaF_2$ at room temperature with a 45±2 nsec lifetime over two decades.

G. Grating formation in impurity doped crystals

The research summarized in this section is a currently ongoing project which is part of the Ph.D. thesis research of David Perry.

Laser-induced-gratings have been used in a variety of experimental techniques to investigate dynamic processes in impurity-ion-doped solids. The simplest of these methods use two laser beams to write a grating in the material and a third beam which Bragg scatters from this grating to measure energy diffusion among the ions as well as study excited state absorption and dispersion. Methods using two simultaneous gratings are used in phase conjugation and degenerate-four-wave-mixing. These gratings are produced by the interference of two laser fields. For two coherent plane waves with equal intensity I_0 and wavelength λ which cross at an external angle $2\theta_e$, the interference pattern is

$$I(x) = 2I_0 [1+\cos Kx] = 4I_0 \cos^2(Kx/2)$$

where $K=2\pi/\Gamma$ is the grating wavevector and $\Gamma=\lambda/2\sin\theta_e$ is the grating period. This modulated intensity couples to the impurity ion system which gives rise to a modulated density of the excited state population.

Recently, we have visually observed this modulation of the excited state population. A 1 mm thick disk of 0.05% Ce^{3+}:YAG was illuminated by two beams from a TE_{00} He-Cd laser operating at 442 nm. This wavelength overlaps the lowest 4f→5d absorption band and excites the Ce ions into the lowest 5d state. The two beams entered the front face of the sample at an external crossing angle of $2\theta_e=1.25°$. A Nikon microscope was used to observe the fluorescence pattern emanating from the back face of the sample. The spatially modulated fluorescence pattern was clearly visible through the microscope. Using a reticule in the microscope eyepiece, we were able to verify a grating spacing of $\Gamma=\lambda/2\sin\theta_e=10.1\mu$.

The fact that we were able to visually observe a well resolved grating pattern through the microscope suggests that there is little energy migration in 0.05% Ce^{3+}:YAG over distances of $\Gamma = 10\mu$. Under cw pumping, the density of excited ions in the grating structure is

$$n(x) \sim 1 + \frac{\cos Kx}{1 + \tau K^2 D}$$

where D is the one-dimensional diffusion constant and τ is the excited state lifetime. For $D \ll 1/K^2\tau$, the grating pattern is not washed out by energy migration among the ions. We are currently pursuing other methods of measuring spatial migration of energy using these grating structures to produce a modulated fluorescence pattern.

With the detailed knowledge we have acquired[20,23] about the excited state processes in Ce^{3+}:CaF_2, we had planned to initiate our investigation with a study of grating formation in this material. In the process of setting up the optical layout for the measurements, the XeCl excimer laser, which generates the 308 nm pump wavelength appropriate for the 4f→5d absorption band in Ce^{3+}:CaF_2, the laser suffered a major breakdown. The failure was traced to a separation of the nickel plating on various components exposed to the reactive halogen gas mixtures which circulate in the laser cavity. The separation of the nickel plating left a bare aluminum surface exposed, which quickly reacted with the chlorine gas mixture. This resulted in a dramatic loss of power and a formation of an aluminum chloride powdery precipitate on the interior widows of the laser. This laser (model EXC-1) was previously purchased with DOE funds, but due to its age, is no longer supported by Quanta Ray/Spectra Physics, the manufacture of the laser. Since we could could not get replacement parts for this laser and since the laser is a major component for these laser-induced grating studies, we have spent some time rebuilding the laser. Replacement parts were machined in both the Physics Department machine shop as well as in the Institute for Materials Science. The parts were all made from a halogen resistant stainless steel which circumvents future plating problems. A total of twelve components were built during the fall of 1987. These included various flange assemblies, fan and bearing mounts as well as gas manifold components. The laser was reassembled in January of 1988, and is now fully operational.

While the excimer laser was being repaired, we began to undertake laser-induced grating measurements by using a pulsed Nd:YAG laser as the pump source instead of the XeCl excimer

laser. The measurements were done using a ruby (Cr^{3+}:Al_2O_3) sample since this material is strongly absorptive at the 532 nm wavelength of the frequency doubled Nd:YAG laser. Moreover, there have been several studies[46,47] of phase conjugation and grating formation in ruby using single-mode cw argon lasers which could be compared to our own measurements. The goal of these initial measurements in ruby was to gain experience in laser-induced grating spectroscopy and to verify that gratings could be created be multi-mode and somewhat incoherent laser sources.

The experimental set-up for these initial measurements is illustrated schematically in Fig. G1. The dielectrically coated beam splitter divides the Nd:YAG laser beam into two beams which are then weakly focussed onto the sample. The path lengths for the two pump beams are equal to within 1 mm, which is less than the coherence length of the YAG laser beam. The crossing angle $2\Theta = 12°$ (in air) gives a spacing of the grating planes of $\lambda/2\sin\Theta = 2.5\ \mu m$, where λ=532 nm is the wavelength of the pump beams. The Bragg condition is met at an angle ϕ where $\sin\phi=\sin\Theta\ (\lambda/\lambda')$, where λ' is the 632.8 nm wavelength of the He-Ne laser probe beam. The first order diffracted beam was detected by a Hamamatsu side-window photomultiplier tube. The time-dependent photomultiplier signal was recorded by a LeCroy transient digitizer and signal averager.

The diffracted beam was seen to vanish whenever one of the two pump beams was blocked, verifying that both beams are required to write the transient grating in the ruby sample. The diffracted signal was observed only when the beam from the He-Ne was incident at an angle which satisfied the Bragg scattering relation. The observed time dependance of the scattered wave was exponential. For a 0.21% Cr^{3+} concentration, the time constant for the decay was 1.7±0.1 msec. This value compares well with the expected value of $\tau/2$ where τ = 3.6 msec is the radiative lifetime of the Cr^{3+} ions. At a 1.2% Cr^{3+} concentration, the grating lifetime drops to 1.2 msec. This reduction is attributed to energy transfer to pair ions and other traps, which in the higher concentration crystals, has a rate comparable to the radiative decay rate. These results confirm that laser-induced gratings can be written using pulsed multi-mode laser sources and that

the time dependence of the scattered wave can be used to characterize the dopant impurity ions of the sample under study.

In addition to creating transient gratings due to a spatial modulation of the excited state density, two laser fields can also be used to create permanent gratings. These permanent gratings arise from a spatially modulated complex index of refraction due to structural or compositional changes in the material. We have recently observed such a permanent grating in Ce^{3+}:CaF_2. The technique used to produce this permanent grating in Ce^{3+}:CaF_2 is illustrated in Fig. G2. The 10 nsec pulse from the XeCl excimer laser uniformly illuminates the center region in a 0.1% Ce^{3+}:CaF_2 sample. A cw He-Cd laser at 442 nm is used to produce the two coherent fields which form a modulated intensity pattern at the sample. A He-Ne laser at 633 nm is used to read the grating via a Bragg-scattering mechanism. The scattered wave is intense enough to be observed visually on a 3x5 white card. The grating is quasi-permanent in that the 633 nm beam slowly bleaches out the grating during the read cycle.

During the grant period, we have investigated the formation of Ce^{2+} in Ce^{3+}:CaF_2 following UV pumping.[20,23] These Ce^{2+} centers are created by electron trapping at a Ce^{3+} ion having O_h symmetry following the two-photon photoionization of a Ce^{3+} ion having C_{4v} symmetry. It is our contention that these Ce^{2+} centers and photoionization processes play a central role in the formation of the permanent gratings in Ce^{3+}:CaF_2. Experiments are planned to attempt to understand the detailed characteristics of the permanent gratings in Ce^{3+}:CaF_2 and related materials.

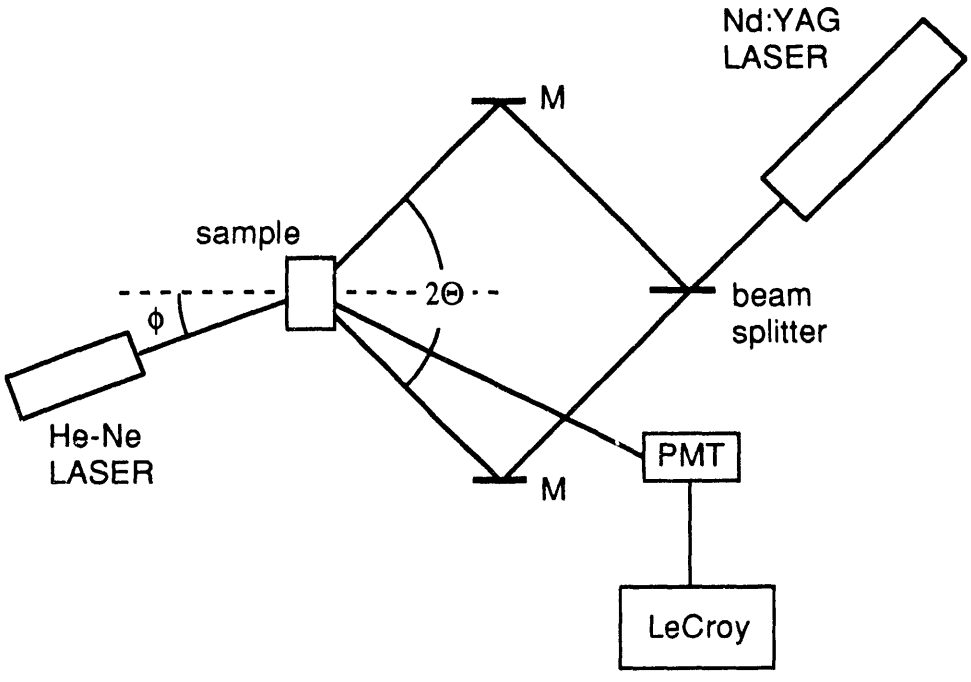

Figure G1. Experimental setup for the laser-induced grating studies. The two beams generated by the Nd:YAG pump laser and create a period modulation of the index of refraction in the sample. The probe beam from the He-Ne laser then Bragg scatters off of the grating. The diffracted beam is then detected with a photomultiplier tube and its time dependance is recorded by the LeCroy transient digitizer and signal averager.

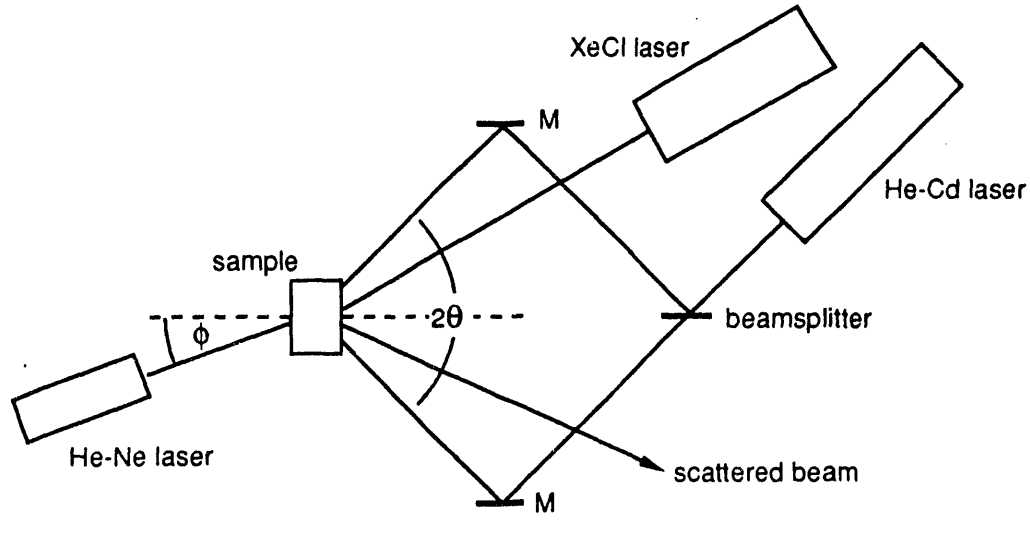

Figure G2. Schematic of the experiment for measuring the characteristics of the permanent gratings in $Ce^{3+}:CaF_2$.

REFERENCES

1. S.K. Gayen and D.S. Hamilton, Phys. Rev. B **28**, 3706 (1983).
2. S.K. Gayen, G.J. Pogatshnik, and D.S. Hamilton, J. Lumin. **31/32**, 260 (1984).
3. S.K. Gayen, Ph.D. thesis, University of Connecticut, 1984.
4. S.K. Gayen, D.S. Hamilton, and R.H. Bartram, Phys. Rev. B **34**, 7517 (1986).
5. C.F. Fischer, Computer Phys. Commun. **4**, 107 (1972).
6. R.M. Sternheimer, M. Blume, and R.F. Peierls, Phys. Rev. **173**, 376 (1968).
7. M. Dagenais, M. Downer, R. Neumann, and N. Bloembergen, Phys. Rev. Lett. **46**, 561 (1981).
8. B.R. Judd and D.R. Pooler, J. Phys. C. 15, 591 (1982).
9. M.C. Downer, A. Bivas, and N. Bloembergen, Opt. Commun. **41**, 335 (1982).
10. J.D.Axe Jr., Phys. Rev. A. **136**, 42 (1964).
11. M.C. Downer and A. Bivas, Phys. Rev. B **28**, 3677 (1983).
12. M.F. Reid and F.S. Richardson, Phys. Rev. B **29**, 2830 (1984).
13. R.R. Jacobs, W.F. Krupke, and M.J. Weber, Appl. Phys. Lett. **33**, 410 (1978).
14. W.J. Miniscalco, J.M. Pellegrino, and W.M. Yen, J. Appl. Phys. **49**, 6109 (1978).
15. J.F. Owen, P.B. Dorain, and T.Kobaysi, J. Appl. Phys. **52**, 1216 (1981).
16. D.S. Hamilton in *Tunable Solid State Lasers* (eds. P. Hammerling, A. Budgor, and A. Pinto), Springer-Verlag, Berlin, 1984.
17. D.S. Hamilton, S.K. Gayen, G.J. Pogatshnik, R.D. Ghen, and W.J Miniscalco, Phys. Rev. B **39**, 8807 (1989).
18. R.D. Ghen, Masters thesis, University of Connecticut, 1986.
19. C. Pedrini, F. Rogemond, and D.S. McClure, J. Appl. Phys. **59**, 1196 (1986).
20. G.J. Pogatshnik, S.K. Gayen, and D.S. Hamilton, J. Lumin. **31/32**, 251 (1984).
21. G.J. Pogatshnik and D.S. Hamilton, J. Lumin. **38**, 201 (1987).
22. G.J. Pogatshnik, Ph. D. thesis, University of Connecticut, 1987.
23. G.J. Pogatshnik and D.S. Hamilton, Phys. Rev. B **36**, 8251 (1987).
24. D.S. McClure and Z.J. Kiss, J. Chem. Phys. **39**, 3251 (1963).
25. R.C. Alig, Z.J. Kiss, J.P. Brown, and D.S. McClure, Phys. Rev. **186**, 276 (1969).
26. A. Winnacker, R.M. Shelby, and R.M. Macfarlane, Opt. Lett. **10**, 350 (1985).
27. D.J. Ehrlich, P.F. Moulton, and R.M. Osgood Jr., Opt. Lett. **4**, 184 (1979).
28. D.J. Ehrlich, P.F. Moulton, and R.M. Osgood Jr., Opt. Lett. **5**, 339 (1980).
29. Ki-Soo Lim and D.S. Hamilton, J. Lumin. **40&41**, 319 (1988).
30. Ki-Soo Lim, Ph.D. thesis, University of Connecticut, 1986.
31. Ki-Soo Lim and D.S. Hamilton, J. Opt. Soc. Am. B **6**, 1401 (1989).

32. G.M. Renfro, L.E. Halliburton, W.A. Sibley, and R.F. Belt, J. Phys. C. **13**, (1980).
33. G.A. Tavshunskii, P.K. Khabibullaev, O.T. Khalikov, and K.B. Seiranyan, Sov. Phys. Tech. Phys. **28**, 513 (1982).
34. Peter Moulton, private communication.
35. W.F. Krupke, M.D. Shinn, J.E. Marion, J.A. Caird, and S.E. Stokowski, J. Opt. Soc. Am **A3**, 102 (1986).
36. A. Suchocki and R.C. Powell, J. Chem. Phys. **128**, 59 (1988).
37. H.S. Kiliaan, A. Meijerink, and G. Blasse, J. Lumin. **35**, 155 (1986).
38. R.S. Meltzer and H.W. Moos, Phys. Rev B **6**,264 (1972).
39. L.J. Andrews in *Tunable Solid State Lasers II* (eds. A.B. Budgor, L. Esterowitz, and L.G. DeShazer), Springer Verlag, 1986.
40. R. Moncorge and C. Pedrini, Excited-state absorption and photoconductivity measurements in Cr^{3+}-doped $LaMgAl_{11}O_{19}$ (Tunable Solid State Lasers Conference, Williamsburg Va., 1987) unpublished.
41. I.M. Bolesta, *et al.*, Sov. Phys. Solid State **28**, 851 (1986).
42. M.J. Weber, Solid State Commun **12**, 741 (1973).
43. H.V. Lauer and F.K. Fong, J. Chem. Phys. **60**, 274 (1974).
44. C. Raptis, J. Phys. E. **16**, 749 (1983).
45. L.L. Chase, S.A. Payne, and G.D. Wilke, J. Phys. C **20**, 953 (1987).
46. D.S. Hamilton, D. Heiman, J. Feinberg, and R.W. Hellwarth, Opt. Lett. **4**, 124 (1979).
47. P.F. Liac and D.M. Bloom, Opt. Lett. **3**, 4 (1978).

III. PUBLICATION SUMMARY (1984-1992, DE-FG02-84ER45056)

A. REFEREED ARTICLES

1. "Laser Induced Defect Centers in $Ce^{3+}:CaF_2$," G.J. Pogatshnik, S.K. Gayen and D.S. Hamilton, J. Lumin. **31/32**, 251 (1984).
2. "Two-photon Excitations of Higher 5d States in $Ce^{3+}:CaF_2$," S.K. Gayen, G.J. Pogatshnik and D.S. Hamilton, J. Lumin. **31/32**, 260 (1984).
3. "Trivalent Cerium as Tunable Laser Systems: Two Bad Apples," D.S. Hamilton, in *Tunable Solid State Lasers*, Vol. 47 of Springer Series in Optical Sciences, ed. by P. Hammerling, A. Budgor and A. Pinto, (Springer-Verlag, Berlin, 1985), pp. 80–90.
4. "Analysis of the Lowest 4f→5d Two-photon Transition in $Ce^{3+}:CaF_2$," S.K. Gayen, D.S. Hamilton and R.H. Bartram, Phys. Rev. B **34**, 7517 (1986).
5. "Excited State Photoionization of Ce^{3+} ions in $Ce^{3+}:CaF_2$," G.J. Pogatshnik and D.S. Hamilton, Phys. Rev. B **36**, 8251 (1987).
6. "Rate Equation Description of Multi-photon Creation of Color Centers and Simultaneous One-photon Annihilation," G.J. Pogatshnik and D.S. Hamilton, J. Lumin. **38**, 201 (1987).
7. "UV-Induced Loss Mechanisms in a $Ce^{3+}:LiYF_4$ Laser," Ki-Soo Lim and D.S. Hamilton, J. Lumin. **40&41**, 319 (1988).
8. "Optical Absorption and Photoionization Measurements from the Excited States of $Ce^{3+}:Y_3Al_5O_{12}$," D.S. Hamilton, S.K. Gayen, G.J. Pogatshnik, R.D. Ghen and W.J. Miniscalco, Phys. Rev B **39**, 8807 (1989).
9. "Optical gain and loss studies in $Ce^{3+}:YLiF_4$," Ki-Soo Lim and D.S. Hamilton, J. Opt. Soc. Am. B **6**, 1401 (1989).
10. "Radiative and Nonradiative Relaxation Measurements in Ce^{3+} Doped Crystals" Li-Ji Lyu and D.S. Hamilton, J. Lumin. **48/49**, 251 (1991).

B. CONFERENCE PRESENTATIONS

1. "Transient Excited State Absorption in Ce^{3+}:YAG," S.K. Gayen, G.J. Pogatshnik, D.S. Hamilton and W.J. Miniscalco, March 1984 Meeting of the American Physical Society, Bull. Amer. Phys. Soc. **II–29**, 538 (1984).
2. "Laser Induced Defect Centers in Ce^{3+}:CaF_2," G.J. Pogatshnik, S.K. Gayen and D.S. Hamilton, International Luminescence Conference, Madison, Wisconsin, 1984.
3. "Two-photon Excitations of Higher 5d States in Ce^{3+}:CaF_2," S.K. Gayen, G.J. Pogatshnik and D.S. Hamilton, International Luminescence Conference, Madison, Wisconsin, 1984.
4. "Trivalent Cerium as Tunable Laser Systems: Two Bad Apples," D.S. Hamilton, Tunable Solid State Lasers Conference, La Jolla, CA, 1984.
5. "UV Laser Induced Photochromic Centers in Ce^{3+}:CaF_2," G.J. Pogatshnik and D.S. Hamilton, March 1986 Meeting of the American Physical Society, Bull. Amer. Phys. Soc, **II–31**, 698 (1986).
6. "Optical Gain Measurements at 325 nm in Ce^{3+}:$LiYF_4$," Ki–Soo Lim and D.S. Hamilton, March 1986 Meeting of the American Physical Society, Bull. Amer. Phys. Soc, **II–31**, 659 (1986).
7. "UV Induced Color Center Formation in Ce^{3+}:$LiYF_4$," Ki–Soo Lim and D.S. Hamilton, March 1987 Meeting of the American Physical Society, Bull. Amer. Phys. Soc, **II-32**, 1420 (1987).
8. "Rate Equation Description of Multi-photon Creation of Color Centers and Simultaneous One-photon Annihilation," G.J. Pogatshnik and D.S. Hamilton, 6^{th} International Conference on Dynamical Processes in Excited States of Solids, Tsukuba Japan, 1987.
9. "UV-Induced Loss Mechanisms in a Ce^{3+}:$LiYF_4$ Laser," Ki-Soo Lim and D.S. Hamilton, International Conference on Luminescence, Beijing PRC, 1987.
10. "$Gd^{3+} \rightarrow Cr^{3+}$ energy transfer and Cr^{3+} decay dynamics in Cr^{3+} doped GSGG, GSAG and GGG," D.S. Hamilton, Li–Ji Lyu, G.J. Pogatshnik, and L.S. Cain, Tunable Solid State Lasers Conference, North Falmouth, MA, 1989.

11. "Optical Properties of Cerium Doped Crystals and Glasses," (invited) , D.S. Hamilton, U.S.–Japan Exchange Seminar on Excited State Dynamics in the Condensed Phase, Honolulu, Hawaii, 1989.
12. "Nonradiative Relaxation Processes in Ce^{3+} Doped Crystals and Glasses," Li J-i Lyu and D.S. Hamilton, March 1990 Meeting of the American Physical Society, Bull. Am. Phys. Soc, **II-35**, 798 (1990).
13. "Excited State Absorption in Ce^{3+} Doped Crystals," (invited), D.S. Hamilton, March 1990 Meeting of the American Physical Society, Bull. Am. Phys. Soc, **II-35**, 616 (1990).
14. "Radiative and Nonradiative Relaxation Measurements in Ce^{3+} Doped Crystals" Li-Ji Lyu and D.S. Hamilton, International Conference on Luminescence, Lisbon Portugal, 1990.

C. THESES

1. Swapan K. Gayen, "Two-photon Absorption Spectroscopy of the Trivalent Cerium Ion in Calcium Fluoride," Ph.D. thesis, University of Connecticut, 1984.
2. Gerald J. Pogatshnik, "UV Laser Induced Photochromic Centers in Cerium Doped Calcium Fluoride," Ph.D. thesis, University of Connecticut, 1986.
3. Ki-Soo Lim, "UV-induced Color Centers and Gain Measurements in Trivalent Cerium Doped Lithium Yttrium Fluoride," Ph.D. thesis, University of Connecticut, 1987.
4. Ronald D. Ghen,"Ground and Excited State Photoconductivity Measurements of Ce^{3+}:YAG," Masters Thesis, University of Connecticut, 1986.
5. Li-Ji Lyu, "Radiative and non-radiative relaxation measurements in cerium-doped crystals and glasses," Ph.D. thesis, University of Connecticut, 1990.

IV. PERSONNEL

During the period 1984 through 1989, this research grant has been used to support six graduate students working on advanced degrees and one undergraduate physics major in the physics department at the University of Connecticut.

Dr. Swapan K. Gayen, who was supported in the first year of this grant, received his Ph.D. in December of 1984 with a thesis titled "Two-photon Absorption Spectroscopy of the Trivalent Cerium Ion in Calcium Fluoride". He then accepted a position as a post-doctoral research associate at the Institute for Ultrafast Spectroscopy and Lasers at the City College of New York with Professor R.R. Alfano. There he worked on picosecond methods for measuring relaxation processes as well as developing Cr:forsterite as a tunable laser material. He is currently an associate professor in the Department of Physics and Engineering Physics, Stevens Institute of Technology.

Gerald J. Pogatshnik completed his Ph.D. thesis entitled "UV Laser Induced Photochromic Centers in Ce^{3+}:CaF_2" in 1986. Dr. Pogatshnik then accepted a position as a staff scientist at the Oak Ridge National Labs where he investigated optical properties of color center laser materials. Dr. Pogatshnik is currently an assistant professor in the Department of Physics, Southern Illinois University at Edwardsville.

Ronald D. Ghen completed a Masters thesis on "Ground and Excited State Photoconductivity Measurements of Ce^{3+}:YAG" in 1986. Mr. Ghen is now at staff scientist at Analysis & Technology, Inc. in North Stonington, Connecticut.

Dr. Ki-Soo Lim completed his Ph.D. thesis on "Transient Optical Gain and Loss Measurements in Ce^{3+}:$LiYF_4$" in 1987. Dr. Lim then accepted a position as a postdoctoral research associate with Professor William M. Yen in the Physics Department at the University of Georgia. There he studied optical properties of solids in restricted geometries and dimensions. He is currently a staff scientist with the Korea Standards Research Institute, Optics Laboratory, Chungnam, Korea.

Dr. Li-Ji Lyu, who was the last student to complete his Ph.D. under the auspices of this grant, completed his thesis on "Radiative and non-radiative relaxation measurements in cerium-doped crystals and glasses" in 1990. He was also been responsible for the lifetime measurements for the Gd→Cr energy transfer investigations. He is currently employed as a staff scientist for CVI Inc.

David Perry was supported by this grant and has been responsible for the initial laser–induced grating spectroscopy and the upconversion spectroscopy work. Mr. Perry has completed his Ph.D. general examinations and his course requirements. He is anticipated to complete his Ph.D. thesis in the spring of 1993.

Sheryll Kelly, who was a senior undergraduate physics major at the University of Connecticut also worked in our research labs. Ms. Kelly completed a senior honors thesis on thermoluminescence spectroscopy, which was an outgrowth of Dr. Pogatshnik's Ph.D. thesis. She is currently employed at Analysis & Technology, Inc. in North Stonington, Connecticut.

DATE
FILMED
12/17/92